AD-A032 994 HARRY DIAMOND LABS ADELPHI MD F/G 17/9
SINGLE-SIDEBAND MODULATOR FOR DOPPLER SIMULATION.(U)
SEP 76 R V GARVER
UNCLASSIFIED HDL-TR-1763 NL

| OF |
AD
A032994

END
DATE
FILMED
1-77

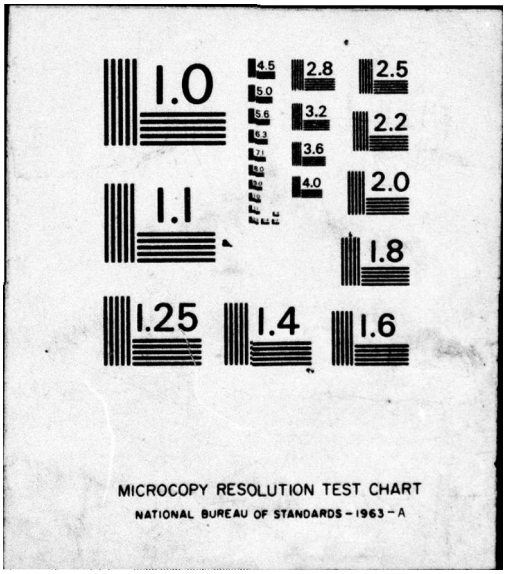
1.0
1.1
1.25
1.4
1.6
1.8
2.0
2.2
2.5
2.8
3.2
3.6
4.0
4.5
5.0
5.6
MICROCOPY RESOLUTION TEST CHART
NATIONAL BUREAU OF STANDARDS - 1963 - A

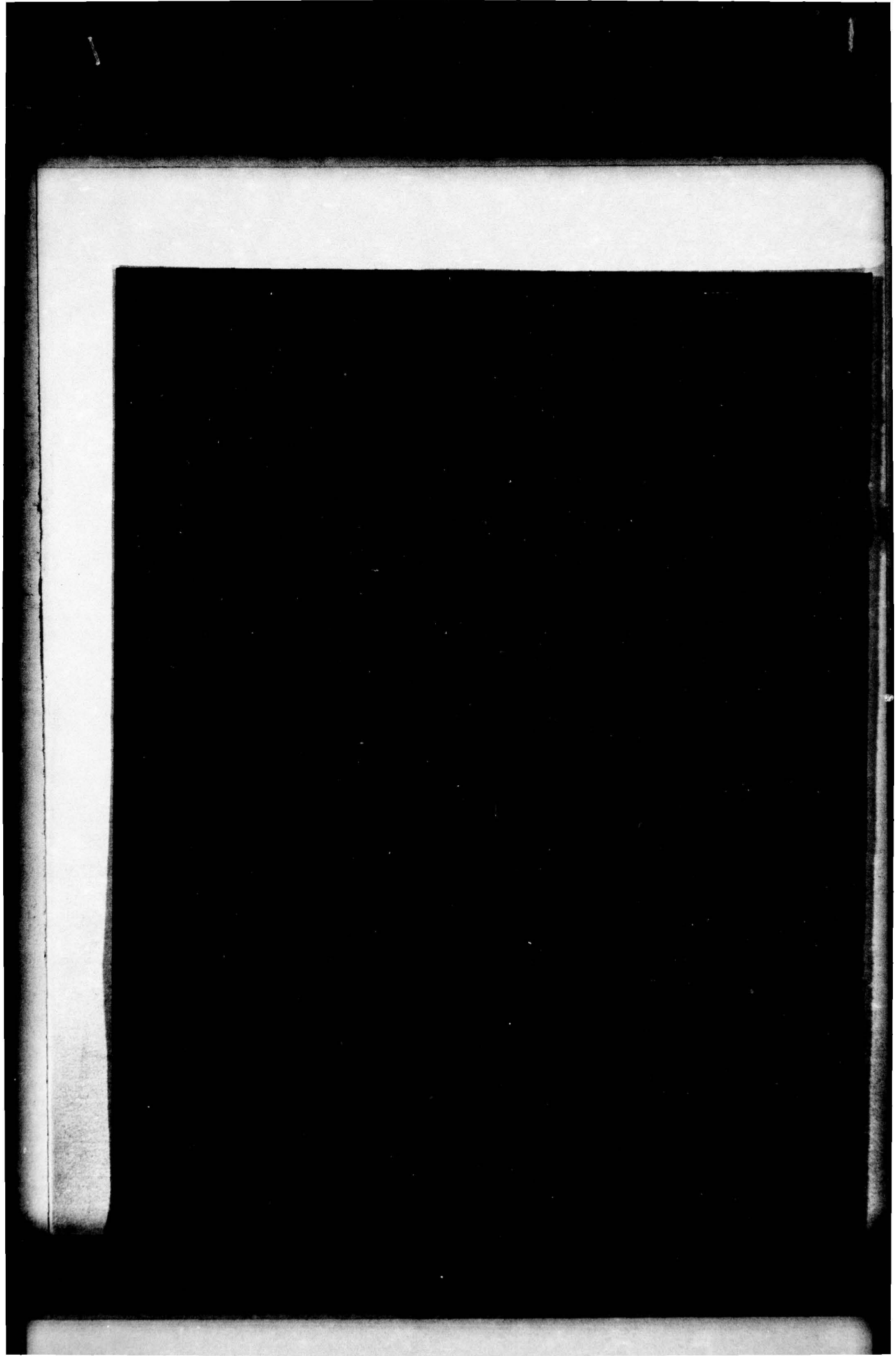

UNCLASSIFIED

SECURITY CLASSIFICATION OF THIS PAGE (When Data Entered)

REPORT DOCUMENTATION PAGE

READ INSTRUCTIONS BEFORE COMPLETING FORM

1. REPORT NUMBER (14) HDL-TR-1763	2. GOVT ACCESSION NO.
3. RECIPIENT'S CATALOG NUMBER (9)	
4. TITLE (and Subtitle) (6) Single-Sideband Modulator for Doppler Simulation,	5. TYPE OF REPORT & PERIOD COVERED Technical Report,
	6. PERFORMING ORG. REPORT NUMBER
7. AUTHOR(a) (10) Robert V. Garver	8. CONTRACT OR GRANT NUMBER(a) (16) DA: 1T061102B14A
9. PERFORMING ORGANIZATION NAME AND ADDRESS Harry Diamond Laboratories 2800 Powder Mill Road Adelphi, MD 20783	10. PROGRAM ELEMENT, PROJECT, TASK AREA & WORK UNIT NUMBERS Program: 6.11.02.A
11. CONTROLLING OFFICE NAME AND ADDRESS US Army Materials Development & Readiness Command Alexandria, VA 22333 (11)	12. REPORT DATE Sept [illegible] 76
	13. NUMBER OF PAGES 63
14. MONITORING AGENCY NAME & ADDRESS(if different from Controlling Office) (12) 61p.	15. SECURITY CLASS. (of this report) Unclassified
	15a. DECLASSIFICATION/DOWNGRADING SCHEDULE

16. DISTRIBUTION STATEMENT (of this Report)

Approved for public release; distribution unlimited.

17. DISTRIBUTION STATEMENT (of the abstract entered in Block 20, if different from Report)

18. SUPPLEMENTARY NOTES

HDL Project: 28325
DRCMS Code: 501B.11.85300

19. KEY WORDS (Continue on reverse side if necessary and identify by block number)

Modulator
Mixer
Doppler
PIN diode
Phaser
lamda

20. ABSTRACT (Continue on reverse side if necessary and identify by block number)

The modulation requirements of a doppler simulator are analyzed in detail. A modulator using two PIN diodes λ/8 apart is described and analyzed. It satisfies the requirements over a broad bandwidth; the conversion loss is independent of the incident power level; and the circuit is inexpensive, simple and noncritical. The performance of the modulator is compared with that of a mixer and with that of a conventional type of single-sideband modulator.

DD FORM 1 JAN 73 1473 EDITION OF 1 NOV 65 IS OBSOLETE

UNCLASSIFIED

SECURITY CLASSIFICATION OF THIS PAGE (When Data Entered)

163 050

mt

CONTENTS

FIGURES

FIGURES

1. INTRODUCTION

Doppler signals provide indications of a moving target and may be used to discriminate against fixed targets. They provide also a convenient method of developing an offset frequency in a system in which the transmitter frequency is used also as the local oscillator frequency. Modulators are required to evaluate these doppler radar systems in the laboratory, in production, and in the field. In the past, this evaluation has involved a wide range of ingenious but expensive devices.

One type of single-sideband (SSB) modulator uses a travelling wave tube (TWT).[1] Application of a sawtooth wave to one of the accelerator grids gives effectively linear phase modulation, which is equivalent to SSB modulation. Equipment available provides about 20-dB gain to the desired sideband and suppression of the carrier and undesired sideband to about 30 dB below the desired sideband. Another version[2] of this modulator uses a varactor linear phase modulator, but this device generally suppresses the carrier and undesired sidebands only about 20 dB. It is also narrow band.

Another SSB modulator uses two balanced mixers (H. Bruns, HDL, private communication) with their outputs phased so that one sideband adds and the other cancels. By use of point contact mixer diodes, this device is sensitive to the level of the input rf power. If hot-carrier

---

[1] *Raymond C. Cumming, The Serrodyne Frequency Translator, Proc. IRE, 45 (February 1957), 175-186.*

[2] *Robert V. Garver, 360° Varactor Linear Phase Modulator, IEEE Trans. Microwave Theory and Techniques, MTT-17 (March 1969), 137-147.*

diodes are used in doubly balanced mixers, the device is insensitive to the input power level. Mixer types of SSB modulators can be made to operate over bandwidths of an octave or more; however, the suppression of undesired sidebands tends to be no greater than 20 dB.

Another device that has been used for SSB modulation uses digital phase modulators.[3] Costs run high because a large number of diodes or ferrite elements is required, and in addition, digital drive circuits are required. Suppressions greater than 20 dB are difficult to maintain.

Single-sideband modulators using frequency down conversion, SSB modulation, and frequency up conversion (L. Tozzi, HDL, private communication) give excellent performance, but a tracking oscillator and other complex apparatus are needed.

All the modulators above, except one, are transmission devices as opposed to reflection devices. The one exception is the diode linear phase modulator. A transmission device is desirable when the system being tested has separate transmit and receive antennas and testing is to be done by direct coupling to the separate antennas. In all other tests, the reflection device is more suitable. A reflecion device is easily converted to a transmission device and vice versa by connecting to a three-port circulator.

---

[3] *Gerald Klein and Leonard Dubrowsky, The Digilator, A New Broadband Microwave Frequency Translator, IEEE Trans. Microwave Theory and Techniques, MTT-15 (March 1967), 172-179.*

Also, it is desirable in an SSB modulator to have the conversion loss to the desired sideband continuously variable to simulate the approaching target. Otherwise, a variable attenuator must be used with the modulator. Of the modulators listed above, the TWT, linear varactor phase modulator, and digital phase shifter versions do not have variable output power level.

The mechanism of interaction between undesired sidebands and desired sidebands in most systems is quite complex. Frequently, the only satisfactory way to prove whether or not some sidebands are troublesome is to try SSB modulators with a given array of sidebands in a test system and observe the variation of radar sensitivity as round-trip path phase is varied. Because of the complexity of the theory and the uncertainty of the measurements, sideband suppression for [illegible]odulators is often specified quite conservatively. This report presents a theoretical derivation of the contribution to errors from the sidebands.

Once the requirements are determined quantitatively, it becomes obvious that some of the overly stringent specifications are relaxed, giving a greater degree of freedom in the design of the modulator. One such requirement is that the carrier be suppressed. When this requirement is eliminated, the construction of an inexpensive SSB modulator having broad bandwidth in a noncritical circuit is facilitated.

2. SIDEBAND SUPPRESSION REQUIREMENTS

This section shows that a conventional amplitude modulator can simulate the doppler when the distance to the mixer from the oscillator is equal for the local oscillator (LO) power and for the signal (Sig) being amplitude modulated. This equality is normally not the case, because the signal being amplitude modulated must pass through several

antennas and connecting transmission lines. The next best situation, then, is to have the two paths differ by an integral number of half wavelengths. This arrangement, however, is sensitive to changes in frequency (as well as phase shifts in the rf paths). When this path length is kept small and operation is restricted to a narrow bandwidth, an amplitude modulator may be quite satisfactory. However, an SSB modulator is insensitive to path length and phase.

2.1 General Considerations

2.1.1 Path Length

Figure 1(a) shows a radar and a simulator connected by antennas. Figure 1(b) shows the circuit simplified, since it is the difference in path lengths of oscillator to mixer that causes sideband errors from all simulator modulators. For a single antenna simulator used with a single antenna radar,

$$\ell_3 = \ell_2 - \ell_1 = \ell \ , \tag{1}$$

and total path length is 2 ℓ.

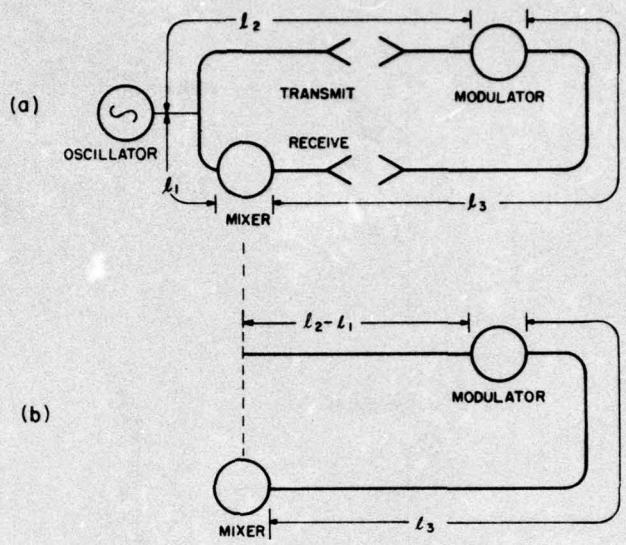

Figure 1. Radar and test chamber.

2.1.2 Modulation Figures

Consider the addition of voltage vectors applied to the mixer diode. To visualize their addition, all voltages are compared with the LO vector; i.e., the angular frequency of the LO is substracted from all vectors so that the LO appears as a vertical vector, a vector for a frequency higher than it rotates counterclockwise at an angular frequency equal to the difference between it and the LO, and a vector for a frequency lower than it rotates clockwise.

Then a signal at the same frequency as the LO adds to the LO voltage applied to the mixer (fig. 2). Angle remains fixed for a constant signal delay. As the distance between the radar and target is reduced, θ becomes smaller continuously, and therefore Sig rotates counterclockwise on LO, inducing a change in mixer current that is sensed as a doppler signal. The magnitude of the mixer output voltage is

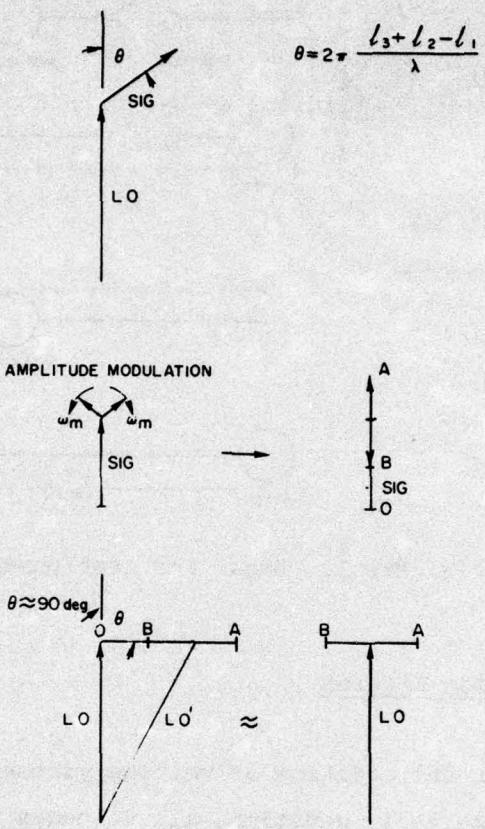

Figure 2. Phaser addition in radar mixer (SIG = signal or simulated signal).

$$V_{mix} = kV_{LO} + kV_{sig} \cos \theta \quad , \tag{2}$$

where $\theta = 4\pi\ell/\lambda$, $V_{sig} << V_{LO}$ (see app A), and where k accounts for the conversion loss of the mixer. Since for this paper kV_{LO} is constant, the only term of interest is $kV_{sig} \cos \theta$, which gives the ac component of the doppler output.

Now consider an amplitude modulator as a doppler simulator. In the plane of amplitude modulation, two sidebands are generated equally above and below the signal (of stationary phase), which give rise to the counterrotating vectors labeled ω_m after amplitude

modulation in figure 2. In this plane, the sum of these vectors produces a Sig vector varying from 0-A to 0-B. When θ = 0 or 180 deg, this produces a maximum variation of the magnitude of the mixer output the same as a doppler signal does. However, when θ = 90 or 270 deg, this modulation figure produces a mixer output voltage that is relatively constant in amplitude. There is no significant simulated doppler signal (and only small harmonic sidebands). Note two things from this construction.

First, when Sig is much smaller than LO, the amount of carrier represented by Sig has little effect on the mixer output. LO becomes LO' (fig. 2). As long as the phase of Sig does not change at the doppler frequency, it alters the effective LO power only slightly. Since the conversion loss of most practical mixers is relatively unchanged by variations in LO power, carrier with the simulated doppler sideband makes practically no contribution to measurement errors. Thus, it is not necessary to require carrier suppression in doppler sideband simulators (unless there is phase modulation in the test path having frequency components in the doppler frequency range).

Second, the fundamental of the simulated doppler signal goes to zero for every odd multiple of quarter wavelengths in differential path length to the mixer; therefore, an amplitude modulator is useful only when electrical path lengths are narrowly enough defined to avoid the nulls. In other words, when the differential path length is small, the oscillator constrained to a narrow frequency range, and the phase shift through the test path tightly constrained, then an amplitude modulator can be used. The modulator has to be very close to the radar to satisfy these conditions in most practical cases.

An SSB modulator does not have modulation nulls. The SSB results in the ω_m vector pivoting on the top of the Sig vector (fig. 3). When this modulation figure is put on the LO vector at 90 deg, the circle of the modulation vector point has the same projection in the LO vector plane as it does at 0 deg or any other phase.

Suppose imperfect SSB modulation were used. The sidebands would be asymmetrical. The AM (equal sidebands) gives a modulation vector point figure that is a straight line. The SSB modulator gives a modulation vector point figure that is a circle. It can be shown (fig. 4) that asymmetrical sideband modulation gives a modulation vector point figure that is an ellipse. The orientation of the ellipse is defined so that beginning point A corresponds to a point on the major axis for maximum signal vector voltage. Instead of nulls at 90 deg, minima occur.

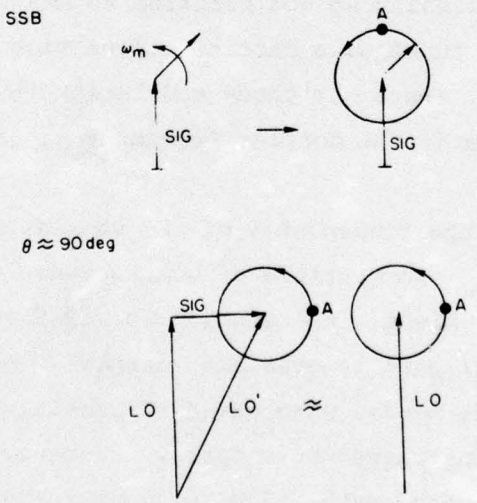

Figure 3. Single-sideband phaser in mixer (SIG = signal or simulated signal).

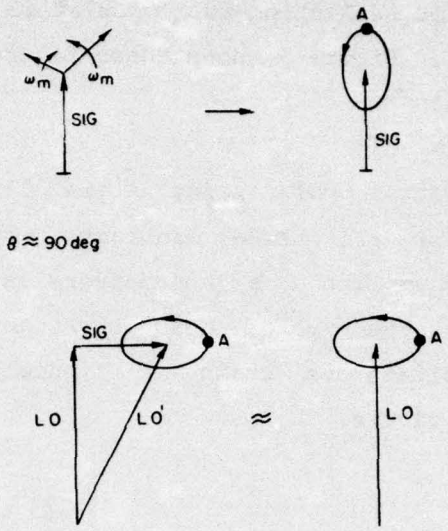

Figure 4. Asymmetrical sideband phasers in mixer (SIG = signal or simulated signal).

This orientation of the ellipse and all subsequent modulation index figures can be done at no sacrifice in generality. The approximation at the bottom of figure 4 shows that aligning the major axis with the unmodulated component of Sig causes no restrictions, because the unmodulated component of the signal is absorbed as a small part of LO. Therefore, point A for all modulation index figures corresponds to that phase for which all modulation index vectors are parallel. This parallel state may never happen when three or more frequencies are present, but it does represent the worst-case conditions when any number of frequencies is present.

These modulation vector point figures are useful conceptual aids for viewing two problems. First, they help in the visualization of the errors caused by undesired sidebands and variations of θ. Second, they permit the direct specification of impedance versus time as plotted

on the Smith chart, for reflection-type modulators (to be used later in designing a modulator). Figure 5 shows these figures for various values of undesired sidebands.

The orientation of point A is determined by θ. For figure 5, θ = 0 deg for all three diagrams. The mixer output is the projection (reduced in amplitude by the conversion loss) of each figure on the vertical axis as the vector head moves counterclockwise around the figure. This voltage is shown in figure 6 for $V_{-2}/V_{+1} = 1.0$ beginning at A on the figure.

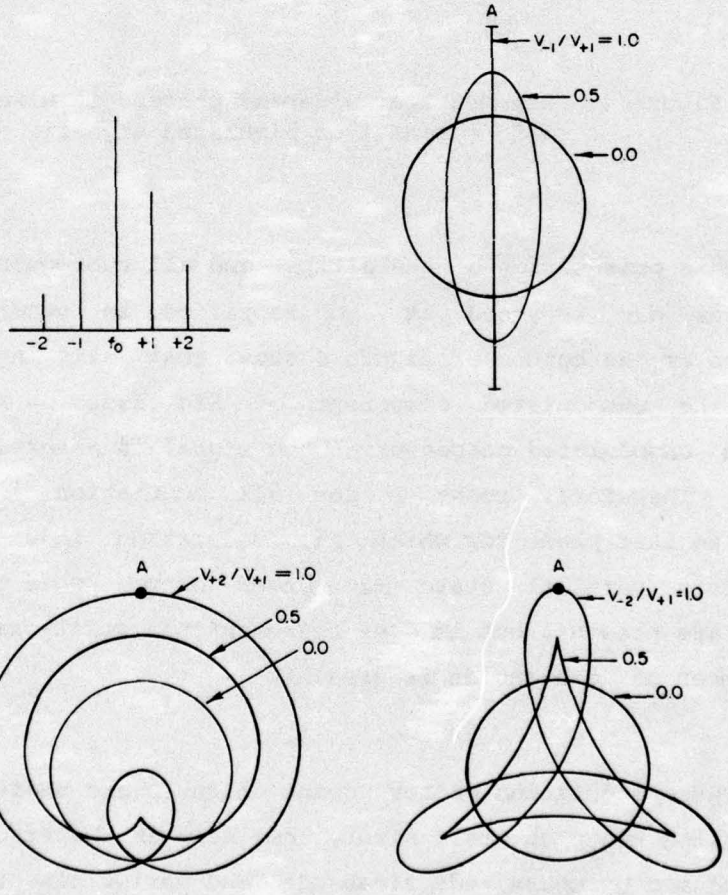

Figure 5. Phaser figures for various sideband combinations.

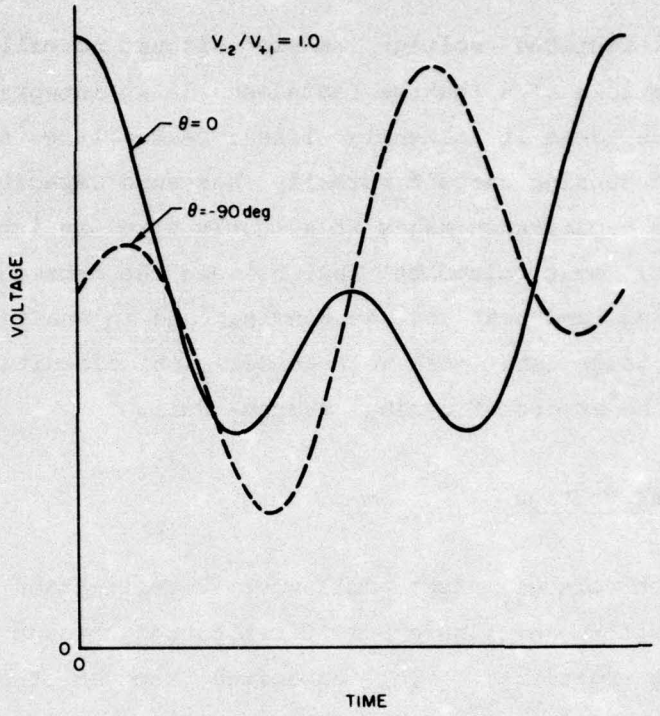

Figure 6. Mixer output with -2 sideband present.

2.2 Information Processing Methods

The suitability of an SSB modulator depends on how much the modulator contributes to errors in system function. Normally, errors are expressed in terms of variation in detected power level, which may be attributed to transmitted power level, antenna gain, and mixer efficiency. However, the important system parameter for an altitude measuring radar fuze is change in function height. Function height depends on the decision circuit. Fortunately, typical system responses fall between the simple cases of integrated voltage sensing and peak voltage sensing.

An integrated voltage sensing circuit normally has a finite memory in the form of a leakage resistance on an integrating capacitor. This resistance makes it slightly like a peak voltage sensing circuit. A peak voltage sensing circuit normally has some capacitance associated with it. This capacitance makes it slightly like an integrated voltage sensor. Thus, most circuits fall between the extremes of integrated voltage sensing and peak voltage sensing; and an analysis of errors in integrated voltage and peak voltage decision circuits gives bounds within which the errors of typical systems fall.

2.2.1 Peak Voltage

Peak voltage after full-wave rectification is considered here. The waveform of figure 6 is first passed through a capacitor and then full-wave rectified. The capacitor removes the dc bias on the mixer output; therefore, the waveform being considered is just the projection of the modulation vector point figures as shown in figure 5 on the vertical axis, 0 V being the center point of each figure.

The +1 sideband is taken to be the desired sideband. Other sidebands are considered in combinations with it. The -1 sideband is considered first with the +1 sideband. The maximum voltage occurs at $\theta = 0$, as shown by the ellipses for V_{-1}/V_{+1} in figure 5, and is given by

$$V_{max} = V_{-1} + V_{+1} \quad . \tag{3}$$

Normalizing gives

$$\frac{V_{max}}{V_{+1}} = 1 + \frac{V_{-1}}{V_{+1}} \quad . \tag{4}$$

Suppression of the -1 sideband is given by

$$S_{-1} = 20 \log \frac{V_{+1}}{V_{-1}} \quad . \tag{5}$$

The error of the response in the mixer is given by

$$\varepsilon = 20 \log \frac{V_{max}}{V_{+1}} \quad , \tag{6}$$

which corresponds to the equivalent error in received signal power level. (In other words, ε = 1 dB could be caused also by the following: the oscillator providing 1 dB more power than wanted, target reflection loss being 1 dB lower than anticipated, antenna gain being 0.5 dB more than wanted, or mixer conversion loss being 1 dB lower than specifications.) By solving equations (4), (5), and (6), the maximum error ε due to the -1 sideband, $\varepsilon_{-1\ max}$, is given by

$$\varepsilon_{-1\ max} = 20 \log \left(1 + 10^{-S_{-1}/20}\right) \quad . \tag{7}$$

The minimum voltage of the -1 sideband occurs at θ = 90 deg and is given by

$$V_{min} = V_{+1} - V_{-1} \quad .$$

Similar to equation (7) above,

$$\varepsilon_{-1\ min} = 20 \log \left(1 - 10^{-S_{-1}/20}\right) . \qquad (8)$$

Now consider the ±2 sidebands. The complex waveforms can be visualized with the aid of figures 5 and 6. The maxima occur at θ = 0 deg and are the same as for the maximum of the -1 sideband. Since a full-wave detector is assumed to precede the peak sensor, the minima from the +2 and -2 sidebands occur when θ = 90 deg. Under this condition, the projection on the LO vector is given by

$$V = V_{+1} \sin \omega_m t \pm V_{\pm 2} \sin 2\omega_m t \ . \qquad (9)$$

By solving for peak voltage,

$$\frac{\partial V}{\partial \omega_m t} = V_{+1} \cos \omega_m t + 2V_{\pm 2} \cos^2 \omega_m t = 0 . \qquad (10)$$

Substituting $\cos 2x = 2 \cos^2 x - 1$ into 10 gives for V_{max}

$$(\omega_m t)' = \cos^{-1} \left\{ - \frac{V_{+1}/V_{\pm 2}}{8} + \left[\left(\frac{V_{+1}/V_{\pm 2}}{8} \right)^2 + \frac{1}{2} \right]^{\frac{1}{2}} \right\} \qquad (11)$$

and

$$\frac{V_{max}}{V_{+1}} = \sin (\omega_m t)' + \frac{V_{\pm 2}}{V_{\pm 1}} \sin 2 \left(\omega_m t\right)' \ , \qquad (12)$$

which combine to give the curves of figure 7. Converting to equivalent error in amplitude gives the curves shown in figure 8. The -1 sideband can give a positive or negative error or any value between the curves.

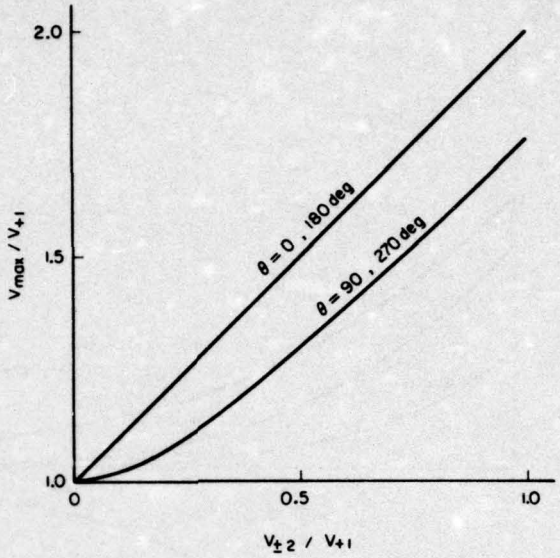

Figure 7. Effective contribution of ±2 sidebands to +1 sideband.

The ±2 sidebands can give a positive error as large as the upper curve or as low as the ±2 minimum peak curve in figure 8. The error from the ±2 sidebands is always positive when only one sideband is present.

The errors for a peak voltage information-processing method become complex when many sidebands are present. However, the maximum possible peak voltage is the sum of all the sideband voltages, and the minimum possible peak voltage is the lowest positive voltage that can be obtained by adding and subtracting the sideband voltages in any combination, but using each one only once. ε_{max} may be expressed

$$\varepsilon_{max} = 20 \log \left| 1 + \sum_{n=-\infty}^{-1} 10^{-S_n/20} + \sum_{n=2}^{\infty} 10^{-S_n/20} \right|. \qquad (13)$$

The limit on ε_{min} is obtained by adding or subtracting the above bracketed terms to obtain the lowest positive number.

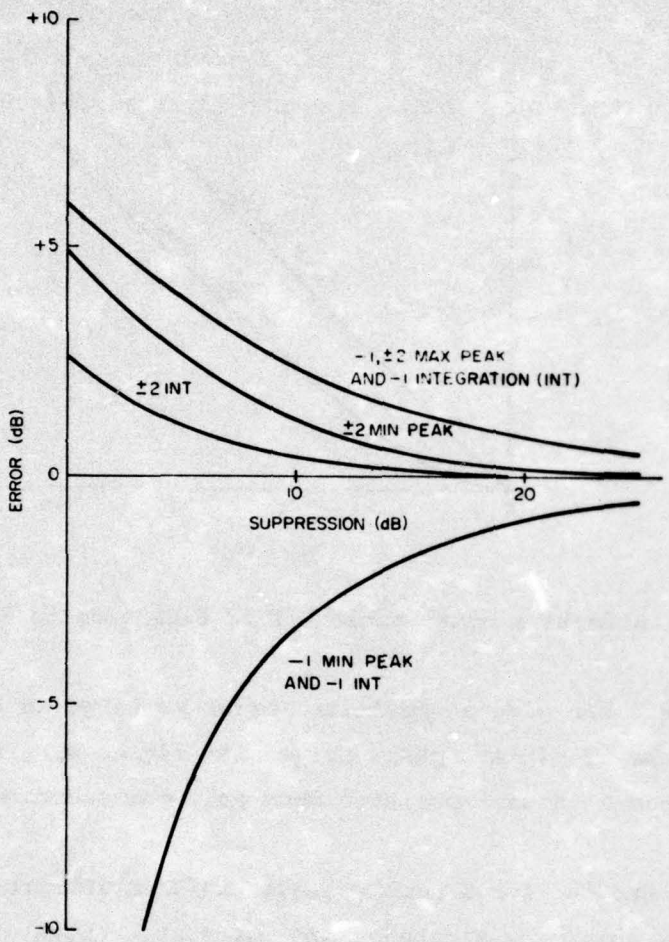

Figure 8. Effective oscillator power change induced by various sidebands.

Referring to figure 8, the equivalent error in returned signal amplitude in a peak voltage information-processing system is ±0.9 dB for 20-dB suppression of the -1 sideband when all other undesired sidebands are negligible; 20-dB suppression of either the +2 or -2 sideband provides +0.9 to +0.2 dB when all other undesired sidebands are negligible.

The electronic circuit representing simple threshold doppler decision circuits is a generator of finite resistance driving a series rectifier diode charging up a capacitor with a finite resistance in

parallel with it. Practical circuits are bounded by two special conditions of this circuit. The first condition is the one having a very small capacitor, in which case the threshold circuit responds to the peak level of the input wave.

The other special condition of the circuit is that of a pure integrator. For this circuit, the resistance in parallel with the capacitor is practically infinite, and the RC time constant of the generator resistance and the capacitance is much, much longer than the longest time required for the capacitor to be charged to the firing threshold voltage. Once the diode begins conducting, the voltage on the capacitor rises slightly, but negligibly, compared to the input signal, because of the long RC time constant. Thus, all parts of the rectified doppler above the conduction threshold of the diode detector contribute to charge on the capacitor. This second condition allows the circuit to be represented as an integrator.

2.2.2 Integrating Voltage

The mixer output voltage of doppler return from a ground plane is inversely proportional to height, h. The normalized voltage on an integrator V_i after full-wave rectification is

$$V_{il} = k_1 \int_h^\infty \frac{|\cos 4\pi x|}{x} \, dx \, , \tag{14}$$

in which k_1, the nominal scaling factor, is determined by oscillator power level, antenna gain, ground reflectivity, and mixer conversion loss--see equation (32). This integral is not easily solved in analytical form; thus, it is replaced by the approximation

$$V_{i1} = k_1 \left[\frac{\int_0^{\pi} \sin x dx}{\int_0^{\pi} dx} \right] \left[\int_h^{\infty} \frac{dx}{x} = k_1 \frac{2}{\pi} \ln x \right]_h^{\infty} . \quad (15)$$

Since this function is indefinite at $x = \infty$, a threshold must be set before integrating (corresponding to the forward conduction threshold of the diode detector), and only the voltage exceeding the threshold is integrated. Integration is set to begin at the height abovegound (H), and the quantity $2k_1/\pi H$ is subtracted from the function before integrating.

$$V_{i2} = k_1 \frac{2}{\pi} \int_h^H \left[\frac{1}{x} - \frac{1}{H} \right] dx = k_1 \frac{2}{\pi} \left[\frac{h}{H} - 1 + \ln \frac{H}{h} \right] . \quad (16)$$

The quantity $k_1 2/\pi[h/H - 1]$ is negative and represents the integral of the voltage below the threshold. This quantity is fixed for a given system setting for a nominal voltage scaler k_1 (and heights). The SSB modulator is going to simulate the external loop loss imperfectly, but not change the system threshold. Therefore, another constant, k_2 (close to unity), is used to represent the departure from the nominal scaling factor in the following equation accurately representing the ideal integrator response.

The proper function (using no approximations) is represented by the following equation (in which k_2 is the normalized voltage):

$$V_{i2} = k_1 \int_h^{\infty} \begin{matrix} \text{pos} \\ \text{part} \\ \text{of} \end{matrix} \left[k_2 \frac{\cos 4\pi x}{x} - \frac{1}{H} \right] dx . \quad (17)$$

Numerical evaluation of this equation showed that equation (16) provided an integrated voltage too high by about $k_1/10$ for H = 100 and H = 1000. The reason is that the smooth continuous function of equation (16) assumes a constant filling factor due to the rectified cosine function. This approximation is acceptable as long as the value of 1/x does not change much over a half cycle of the cosine function, the approximation being most accurate at great distances. However, the subtraction of the threshold voltage disturbs this approximation by permitting only short pulses of voltage to be integrated at great distances, which is less than a constant filling factor.

The object of the calculations is to determine the error introduced by the undesired sidebands when height sensing is done with an integrated voltage decision circuit. Since the peaks due to the desired sideband render the simple analytic equation (16) inaccurate, the peaks due to the ±2, etc., sidebands are even shorter and similarly add even greater errors. Thus, computer simulation is used to determine errors caused by the sidebands.

The -1 sideband produces the same doppler frequency when added to the +1 sideband as the +1 sideband does alone. Thus, the presence of the -1 sideband alters the magnitude of signal k_2 the same as it does for peak voltage sensing circuits. Because the peak pulses at great distances are the same, it produces the same errors as shown in figure 8. The error in figure 8 is equivalent to change in k_2, which corresponds to deviations from the nominal in oscillator power or loop loss.

If the integrator had no threshold subtraction before it, then the ±2, ±3, etc., sidebands would add directly to the integrated voltage (with the approximation that the function did not change much in a half cycle). The error due to any one of these higher-order sidebands would be the same as shown by the curve labeled "±2 max peak" in figure 8. The decision circuit does not function without uncertainty unless the threshold voltage is used. The peak pulses at great distances for the higher-order sidebands also differ from those for the -1 sideband. To interpret the errors of these higher-order sidebands, a more specific system has to be considered.

Figure 9 shows the normalized integrated voltage of a doppler system approaching ground as simulated on the computer. The threshold was set so that integration should begin at 1000 wavelengths. The normalized integrated voltage is shown as a function of height

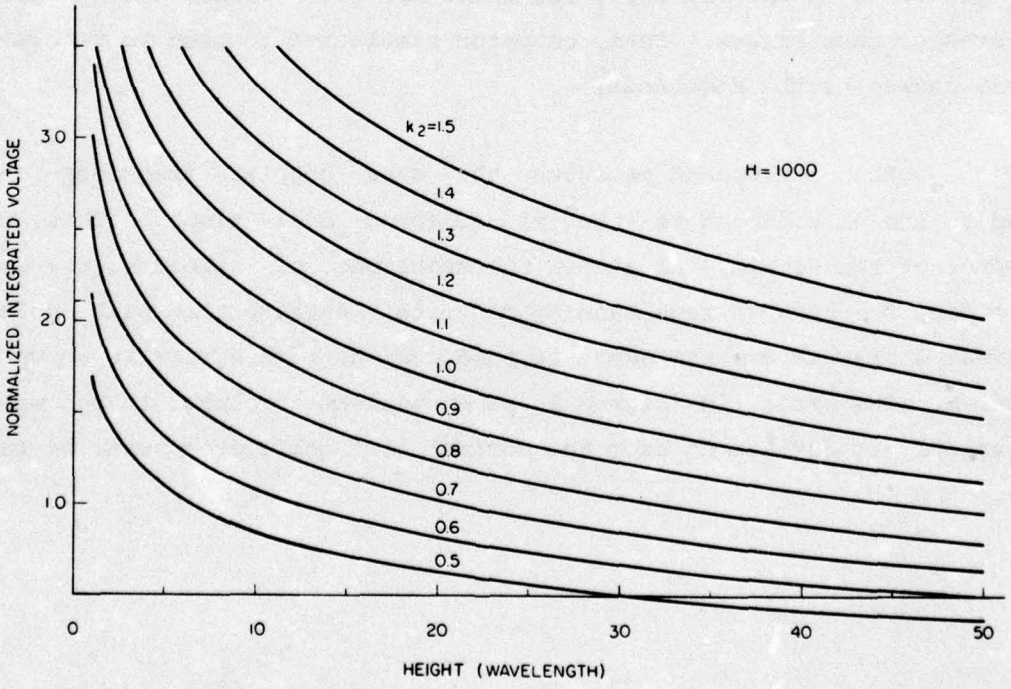

Figure 9. Normalized integrated voltage changing oscillator voltage.

aboveground and normalized oscillator voltage. Assuming that the desired function height is 10 wavelengths, the various function heights from different oscillator voltages can be determined for a constant integrated voltage (in fig. 9, 2.12).

The curves of figure 9 are reduced to the single curve for H = 1000 in figure 10. Oscillator amplitude fluctuation is shown in decibels instead of voltage to relate more directly to the factors contributing to the errors: oscillator power level, antenna gain, ground return loss, and mixer conversion loss, all normally characterized in units of decibels. The curve for H = 100 is derived in the same manner as that for H = 1000. The straight dashed line for peak detection decision circuits comes from the direct proportionality between oscillator voltage and peak detected voltage. Threshold voltages in front of peak detectors cause their responses to be nonlinear and approach the curves for integrators. Leakage resistors

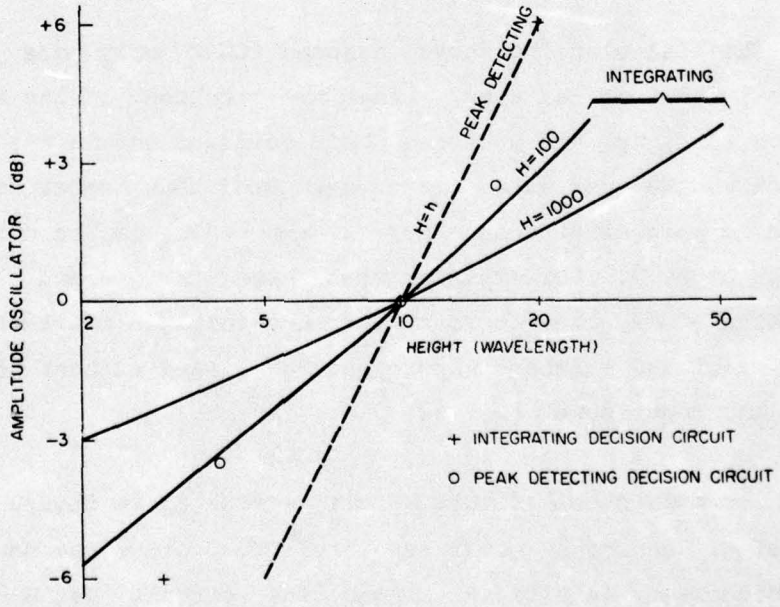

Figure 10. Function height versus oscillator power for various decision circuits.

that are put across the storage capacitors of integrators cause their responses to approach the straight line for peak detectors; practical responses lie somewhere between the curves shown in figure 10. The normalized responses of two development decision circuits are shown as data points in figure 10. Although V_i in equation (16) was $k_1/10$ too high for the simulated data, the equation reproduces the solid curves shown in figure 10 within about 10 percent for $h > 3$.

The response of the +2 sideband was simulated as in figure 9, but for H = 100, and compared with the curves for V_{+1}. For example, the curves for $V_{+1} = 1.0$ and $V_{+2} = 0.5$ lie practically on top of the curve for $V_{+1} = 1.1$ (which also corresponds to the maximum of $V_{+1} = 1.0$ and $V_{-1} = 0.1$). Thus, $V_{+2} = 0.5$ contributes the same error as an oscillator voltage level change by 1.1 or +0.83 dB. $V_{+2} = 0.5$ corresponds to a suppression of 6 dB; thus, the curve for "± 2 integration" on figure 8 was generated.

The calculations have assumed that only one undesired sideband is present at a time. When two sidebands of the same order, but of opposite signs, are present, their voltages add in the worst case and subtract in the best case. It is estimated that higher order than 2 contributes no more error than order 2 and thus can be considered in pairs as was order 2. For example, when both the +2 and -2 sidebands are suppressed 30 dB, then at worst they add voltages providing the same error as a single +2 sideband suppressed 24 dB, and at best they cancel each other and contribute no error.

The curves of figure 8 are rearranged in figure 11 to show the level of -1 sideband power required to produce the same positive errors. When the circuit is an integrating circuit (at H = 100), the equivalent error is given by the curve for integration. The error is no more and no less. As the circuit approaches peak detection in its

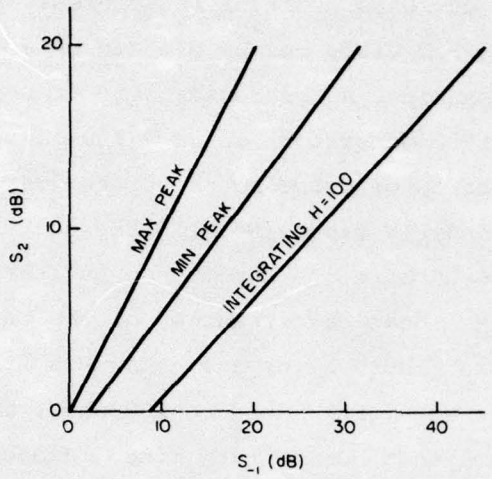

Figure 11. Effective suppression of -1 sideband resulting from ±2 sidebands.

response, the error can range up to the peak maximum line. The general statement can be made that each higher-order sideband contributes no more to error than the -1 sideband, and usually each one contributes less.

3. PIN DIODE MODULATOR

3.1 Circuit Operation

A PIN diode is a current-controlled resistor. More accurately, a PIN diode is a current-controlled conductor, since the diode conductance is approximately proportional to current. In a typical microwave PIN diode, the rf conductance is given approximately by

$$g_{rf} = 75\ I_{dc},$$

in which I_{dc} is the dc bias current in amperes. Ignoring parasitics, the admittance of a PIN diode may be plotted on a Smith chart as shown in figure 12(a), assuming a characteristic impedance of 100 ohms. Moving $\lambda/8$ toward the generator in a 100-ohm transmission line transforms the admittance of diode No. 2 to the vertical line shown in figure 12(b). A second PIN diode (No. 1) like the first added in this electrical plane would have the admittance by itself as shown by No. 1 in figure 12(b). The total admittances of the two diodes in the same electrical plane as in figure 12(b) are shown in figure 12(c). For the vertical line, diode No. 1 is biased to 100 ohms, and the bias on diode No. 2 is varied. For the horizontal line, diode No. 2 is biased to 100 ohms, and the bias on diode No. 1 is varied. To obtain the dashed circle shown in figure 12(c), the two diodes are driven in quadrature by modified sine waves. When a perfect circle is drawn, the voltage of the reflected wave can be represented by fixed vector Γ_c from the center of the Smith chart to the center of the circle, plus rotating vector Γ_{SB} equal to the radius of the circle as shown in figure 13. Γ_c represents

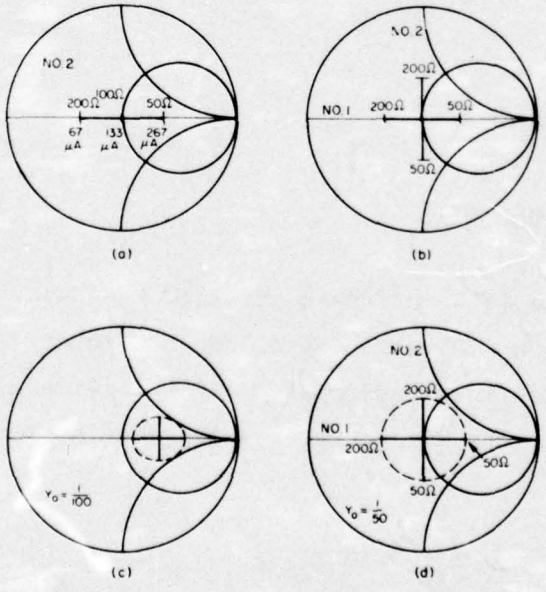

Figure 12. Normalized admittance of PIN diodes being added $\lambda/8$ apart.

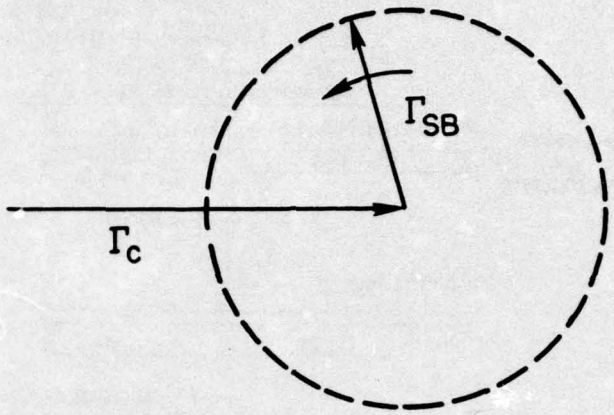

Figure 13. Reflection coefficient vectors showing how single-sideband modulation is obtained.

carrier voltage reflected (at the carrier frequency), and Γ_{SB} represents sideband voltage reflected (at a frequency slightly higher than the carrier). If the circle were perfect and equal time increments provided equal arcs, no other sidebands would be present. However, the reflection coefficient of a PIN diode is a nonlinear function of voltage or current drive, and the admittance adding process in the microwave circuit introduces further nonlinearities. Thus, other sidebands are present.

When the diode pair giving the admittance shown in figure 12(c) is mounted on a 50-ohm transmission line instead of a 100-ohm transmission line, the result is shown in figure 12(d). The magnitude of the reflected carrier is reduced to zero, and the magnitude of the sideband is increased. The circuit can be embodied in strip line as shown in figure 14. Only the center strips are shown. The 25-ohm open circuit stubs provide rf ground to one end of each diode, suppress rf leakage out the modulation ports, and permit the application of dc and modulation voltages to the diodes. The 100-ohm stub to ground provides dc return for the diode driving currents without interfering with rf operation. A dc voltage is needed to bias each diode to the 100-ohm operating point. This simple circuit is a reflection-type SSB

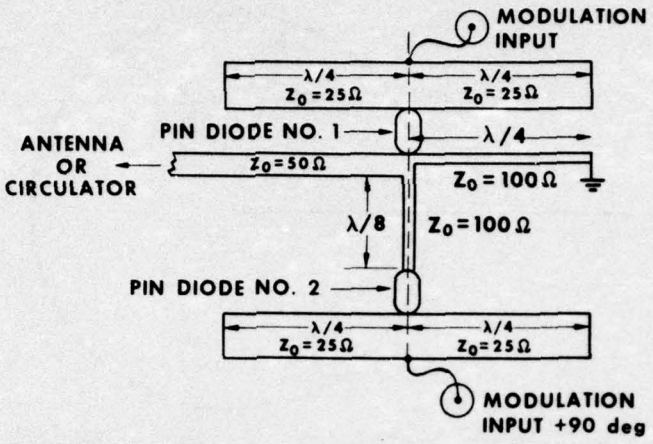

Figure 14. Strip-line circuit layout for PIN diode single-sideband modulation

modulator. Conversion loss is independent of incident power level up to about 100 mW, because the PIN diode is a poor rectifier--the rf impedance is determined primarily by the modulation input power. Although it will not be proved analytically, it has been demonstrated with computer simulations and on working devices that changes in the conversion loss in decibels are equal to changes in the modulation power in decibels. Thus for a fixed input power level, a modulation signal can be translated directly in frequency and power into the desired sideband. Recall from section 1 that TWT serrodyne and digital and linear phase shifters needed an additional control element for amplitude control. The variable attenuator, which had to be used with them for the amplitude control, usually created problems when it was used with these other devices, because it had to be well matched to prevent phase nonlinearities that in turn would induce undesired sidebands. The SSB modulator of figure 14 is so simple that all that is needed to test doppler systems is an antenna connected to the 50-ohm line and a bias circuit and a combination of modulation splitter and 90-deg phase shifter connected to the modulation input ports.

The derivation thus far has assumed that the PIN diode has no parasitics. It has parasitics that can be approximated by the equivalent circuit of figure 15. Typical values of the elements for a glass-packaged diode are given by

$$R_s \approx 2 \text{ ohms},$$

$$L_w \approx 3.7 \text{ nH},$$

$$C_c \approx 0.0 \text{ pF},$$

$$C_d \approx 0.2 \text{ pF},$$

$$\alpha_{rf} \approx 75.$$

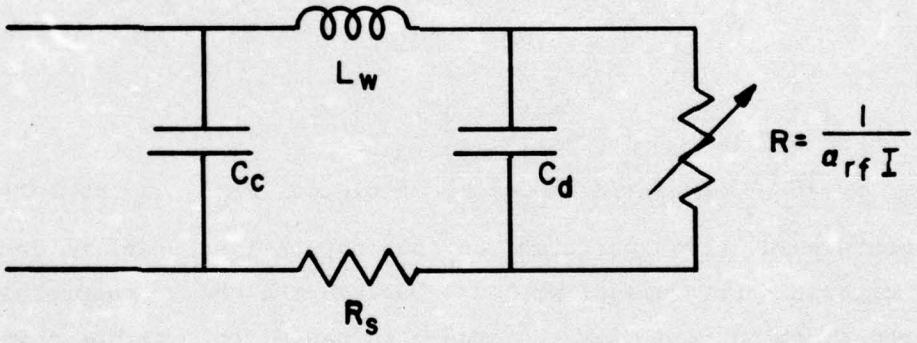

Figure 15. Equivalent circuit of PIN diode.

The admittance at 1 GHz normalized to 100 ohms for a diode having these parameters is shown in figure 16. Although the impedance of the diode no longer gives a horizontal line, it is nevertheless nearly straight, and a second diode $\lambda/8$ away from the first provides a second line perpendicular to the first. Thus, the circuit still provides the necessary orthogonal admittance addition needed to generate a circle on the Smith chart.

Because of the two nonlinearities in the PIN-diode SSB modulator, an analytic approach to the design was not attempted. A model for the modulator was constructed on the digital computer.

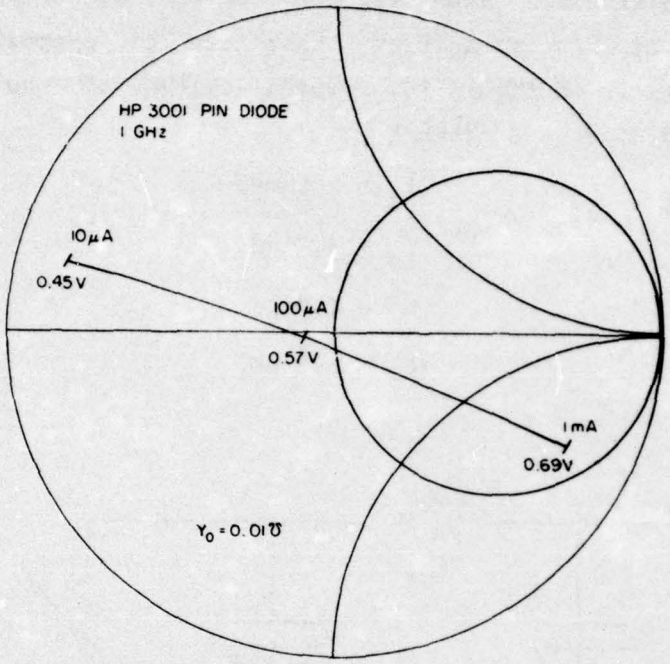

Figure 16. Normalized impedance of typical PIN diode at 1 GHz.

Experiments were then performed on the computerized model to determine which circuit arrangement would provide the best suppression of undesired sidebands and give the greatest bandwidth. At the completion of the computer work, numerous experimental models were built to verify the computer results. Variations that were easy to make on the experimental model, but not easy to make on the computer model, resulted in some improvements not forecast by use of the computer model.

3.2 Sideband Analysis Method

The computer was used to calculate numerically the circuit admittance points much as was done for figure 12. The rf admittance of the diodes depends on the low-frequency current, I, through them given by

$$I = I_o \left(e^{\alpha_{dc} V} - 1\right) \simeq I_o e^{\alpha_{dc} V}, \quad \text{for } I >> I_o ,$$

in which $I_o = 3.4 \times 10^{-9}$ A and $\alpha_{dc} = 20V^{-1}$. The contribution of R_s to the modulation waveform was neglected. The circuit of figure 17 was used to represent the modulator in calculating the input admittances.

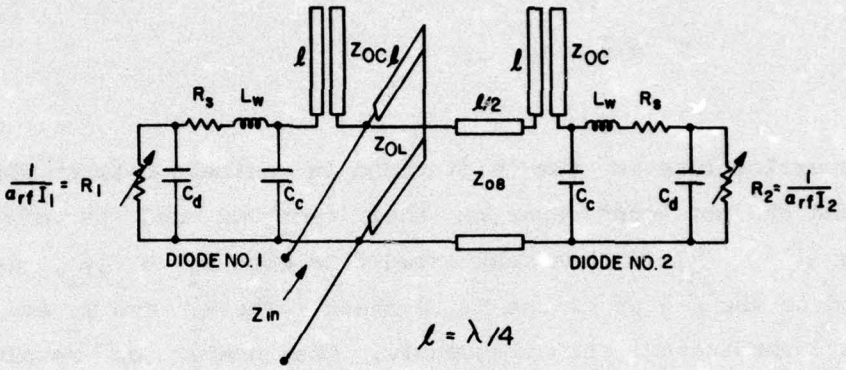

Figure 17. Equivalent circuit of complete single-sideband modulator.

The input reflection coefficient Γ_{in} was calculated assuming that the circuit of figure 17 terminates a 50-ohm transmission line.

$$\Gamma_{in} = \left| \frac{0.02 - Y_{in}}{0.02 + Y_{in}} \right| \tag{18}$$

Sinusoidal voltage drive was assumed for the computer work. A 50-ohm source was used for experimental work. Brief computer use of current drive showed slightly less (≈1 dB) suppression of the highest level of undesired sidebands.

Since the sidebands can be found directly in the Γ plane, they were subtracted out one by one. For one full cycle of modulation, 36 evenly spaced points were used. Each point has an x_i and y_i coordinate in the Γ plane. The voltage of the sideband for which the Smith chart is standing still is equal to the vector from the center of the Smith chart to the centroid of the 36 points, which is obtained by finding the center of gravity of the evenly spaced points.

$$\bar{x} = \frac{1}{36} \sum_{36} x_i \ ,$$

$$\bar{y} = \frac{1}{36} \sum_{36} y_i \ , \qquad (19)$$

$$\Gamma_n = \bar{x} + j\bar{y} \ .$$

The conversion loss is the difference in decibels between the incident power and the reflected power at that sideband and is given by CL = $-20 \log |\Gamma_n|$. Γ_n is then subtracted from each $x_i + jy_i$, moving the centroid to the center of the Smith chart. The x_i and y_i are converted to polar coordinates. Simultaneously, the number of revolutions is counted (q), and the direction of rotation is sensed (indicating which sideband is the largest remaining). The data points are then converted to this new frequency by subtracting $iq(2\pi/36)$ from the angle of each point. This procedure was repeated until all sidebands with conversion loss less than 80 dB had been removed. This sideband-subtraction method of Fourier analysis has the advantage that it calculates the largest sidebands first and ignores smaller sidebands.

The sideband subtraction method is normally far more effective than Fourier transforms when both amplitude modulation and phase modulation are present. Normally, the Fourier transforms of the amplitude modulation and phase modulation are found separately, and their joint contribution to sidebands is found by taking lengthy convolutions.

A newer method for evaluating the sidebands is to take the Fourier transforms of the projection of the points on the x axis and on the y axis, obtaining

$$x = a \cos\left(\omega_m t\right) - b \sin\left(\omega_m t\right) \ ,$$

$$y = c \cos\left(\omega_m t\right) + d \sin\left(\omega_m t\right) \ . \qquad (20)$$

The magnitude of the m sidebands $A_{\pm m}$ is

$$A_{\pm m} = \left[\left(\frac{a \pm d}{2}\right)^2 + \left(\frac{c \pm b}{2}\right)^2\right]^{\frac{1}{2}} \ . \qquad (21)$$

This last method of finding the sidebands should be even faster than the first method by use of Fast Fourier transforms.

3.3 Computer Results

The first computer results did not include all of figure 17 in the circuit. Not included were Z_{OL}, Z_{OC}, C_c, L_w, and C_d. Also, Z_{08} = 100 ohms. The diodes were biased to 100 ohms and driven between

$$\bar{G}_{max} = \frac{G_{max}}{0.01}$$

and

$$\bar{G}_{min} = \frac{1}{0.01\ G_{max}} \ . \qquad (22)$$

The conversion loss to the various sidebands is shown in figure 18. The +1 sideband is taken to be the desired one. All conversion losses are related in decibels to the incident power level. To simplify notation, CL_{+1} is used to denote the conversion loss in decibels to the desired sideband, and CL_{+2} is the conversion loss of the +2 undesired sideband.

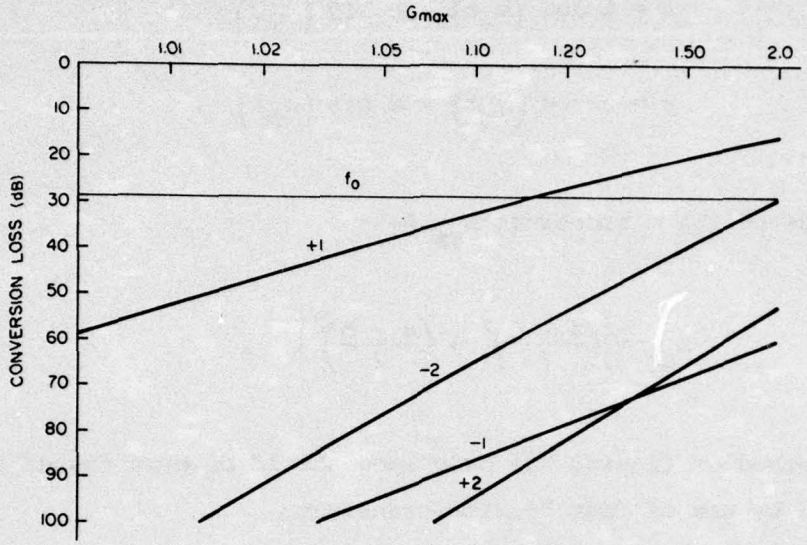

Figure 18. Conversion loss as function of drive.

Suppression S_n is defined as the difference in decibels between the conversion losses of an undesired sideband and the desired sideband. From a large number of curves such as in figure 18, the following general statements can be made concerning sideband levels of the PIN-diode SSB modulator:

a. When the behavior of three sidebands is known, the others can be calculated from it.

b. These three sidebands are f_o, +1, and -1.

c. The other sidebands can be determined from the following equations:

$$CL_{-2} = 2CL_{+1}\ , \qquad CL_{+2} = CL_{-2} + CL_{fo}\ ,$$

$$CL_{-3} = \frac{10}{3} CL_{+1}\ , \qquad CL_{+3} = CL_{-3} + CL_{fo}\ . \tag{23}$$

No sidebands depend on CL_{-1}. As far as observed, the conversion loss of the -n sideband is given by

$$CL_{-n} \simeq n \frac{10}{9} CL_{+1} , \tag{24}$$

and that of the +n sideband is given by

$$CL_{+n} \simeq CL_{-n} + CL_{fo} . \tag{25}$$

Summarizing the sideband conversion loss,

a. The conversion loss of the desired sideband, +1, sets the conversion loss of all the -n sidebands (except -1) directly and of the +n with the aid of the f_o.

b. The f_o conversion loss helps set the conversion loss of the +n sidebands (except +1).

c. The conversion loss of the -1 sideband neither is set by others nor sets others.

Therefore in the succeeding analysis only, the conversion loss of +1, f_o, and -1 sidebands are shown, since all others can be calculated from them.

As another important point to be noted from figure 18, a 20-dB increase in drive reduces conversion loss by 20 dB. Since the diode is biased to $\bar{G}_{max} = 1.0$, the horizontal axis of figure 18 is proportional

to modulation power expressed in decibels. The conduction of the diode is proportional to the current, and the power in decibels is 20 times the log of the current. $\bar{G}_{max}$ = 1.01 gave 53.07 dB, and 1.1 gave 33.45 dB. Thus, 20-dB increase in drive produced 19.62-dB decrease in conversion loss. Experimental work with a 50-ohm modulator (instead of a 0-ohm source as assumed for the computer model) provided less than 1-dB deviation from linearity for greater than 10-dB conversion loss. This linearity between drive power and sideband conversion makes it possible to transfer energy into the sideband proportional to the low-frequency drive.

Ideally, the transmisssion-line sections of figure 17 may be adjusted so that they do not limit the bandwidth. The Z_{OL} line may be a fine wire with ferrite beads on it to approach $Z_{OL} = \infty$. The Z_{OC} line may be made on thin dielectric material to approach $Z_{OC} = 0$. And the Z_{08} line may be replaced by two complementary lines, one having several C sections to provide a constant, frequency-independent, 45-deg differential phase shift between the diodes referenced to the admittance adding point (Schiffman phase shifter).[4] The modulator would then work over extremely wide bandwidths, limited only by the diode parasitics.

The three reactive elements representing the diode parasitics have the structure of a low-pass filter. Furthermore, C_c may be increased to improve performance, since it was 0 pF for the Hewlett-Packard (HP) 3001 diode used in the experiments and simulated in the computer program and since it appears at the available terminal of the diode. The low-frequency characteristic impedance of the diode parasitics Z_{op} is given approximately by

---

[4] *B. N. Schiffman, A New Class of Broad-Band Microwave 90-Degree Phase Shifters, IRE Trans. Microwave Theory and Techniques, MTT-6 (April 1958), 232-237.*

$$Z_{op} = \left(\frac{L_w}{C_c + C_p} \right)^{\frac{1}{2}} . \tag{26}$$

Making $C_c = C_o = 0.2$ pF to make an equal ripple low-pass structure gives $Z_{op} = 96.3$. This should give about a 0.002-dB ripple up to about 4 GHz in a 100-ohm transmission line. For low-insertion-loss ripple,

$$\omega_c \simeq \frac{1}{\left[L_w \left(C_c + C_o \right) \right]^{\frac{1}{2}}} . \tag{27}$$

A 0.002-dB insertion loss from reflections causes a return loss of 36 dB. Two of these reflections 90 deg apart in the Γ plane should give a 33-dB return loss. Computer simulations give f_o down 33 dB up to 3.3 GHz for $C_o = 0.2$ pF. Thus, the above figures are not exact, but give a good estimate of the bandwidth possible from a diode whose parasitics are known.

The bandwidth possible for the HP 3001 having various values of C_c is shown in figure 19. It was shown in section 1 that the conversion loss of f_o was not important; therefore, it is not shown in figure 19. As a practical matter, it is difficult to maintain the return loss of f_o much below 20 dB over any bandwidth, due to other mismatches in practical strip-line circuits. A return loss of 20 dB corresponds to an input VSWR of 1.2. The conversion to the sidebands is influenced by CL_{fo} only in addition to some factor times CL_{+1}. Thus, the only remaining troublesome sideband is the -1 sideband. Figure 19 shows the conversion loss of the -1 sideband when the conversion loss to the +1

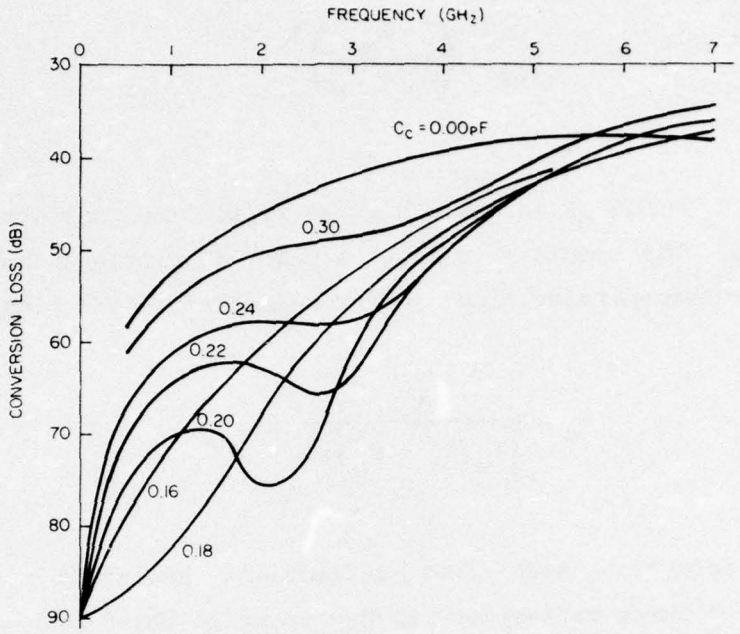

Figure 19. Improvement of bandwidth by increasing C_c of CL_{-1} (CL_{+1} = 30 dB).

sideband is 30 dB. For C_c = 0.2 pF, $S_{-1} \geq$ 33 dB up to 2.9 GHz. An addition to C_c increases the conversion loss of the -1 sideband as well as that of f_o. CL_{fo} was 25 to 30 dB less than CL_{-1} for all cases shown in figure 19.

The information in figure 19 is useful also for narrow-band designs. The conversion loss of the -1 sideband at the center frequency is as shown in figure 19. At 30-dB conversion loss, the conversion loss of the -1 sideband is greater than 70 dB up to 2.6 GHz with C_c = 0.2 pF, greater than 60 dB up to 3.2 GHz with C_c = 0.22 pF, and greater than 50 dB up to 4 GHz with C_c = 0.24 pF. Thus, this inexpensive diode can be used quite well up to significantly high frequencies. Diodes with lower parasitics could be used to higher frequencies if either (1) the characteristic impedance of the parasitic network matched the lines to which the diodes were connected or (2) the cutoff frequency were so high that the reactive contribution of the parasitic network did not deteriorate -1 sideband conversion loss.

Suppose that a constant differential phase-shift network is used between the diodes and the admittance-adding point, but that Z_{OC} and Z_{OL} are allowed to have more easily realizable values than previously. Figure 20 shows the conversion loss of the carrier, fo, and conversion loss of the -1 sideband for C_c = 0.2 pF and CL_{+1} = 30 dB. CL_{-1} depends on Z_{OC} and not on Z_{OL}. For $Z_{OL} = \infty$, CL_{fo} is 25 dB less than CL_{-1}, but for $Z_{OL} \leq 160$ ohms, CL_{fo} is substantially independent of Z_{OC} and dependent only on Z_{OL}. Based on figures 19 and 20, the general statement can be made that CL_{-1} depends mainly on the effects of elements separating the diode variable resistances from the summation point, and CL_{fo} depends mainly on the effects of elements between the summation point and the observation point. CL_{+1} was changed only when CL_{fo} became so low that it reduced power getting to the nonlinear resistances. For example, when CL_{fo} is 10 dB, 10 percent of incident power is reflected, and CL_{+1} deteriorates by about 0.5 to 30.5 dB.

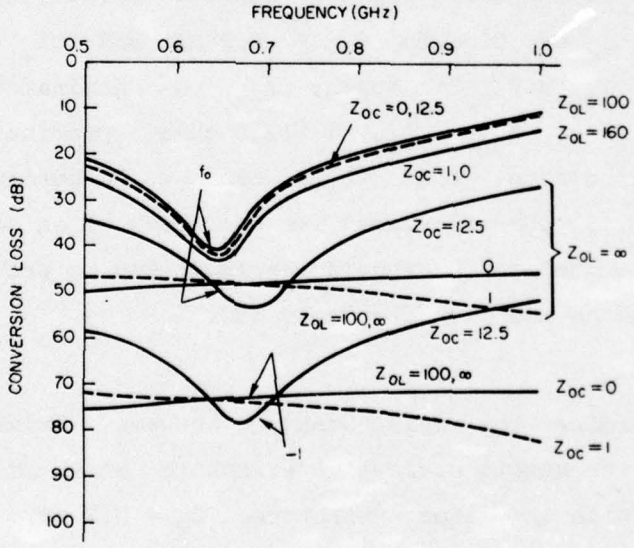

Figure 20. Conversion loss contributions of Z_{OL} and Z_{OC}.

To determine the contribution of the Z_{08} line section, set $Z_{OC} = 0$, $Z_{OL} = \infty$, $Z_{08} = 100$ ohms, $C_c = 0.2$ pF, and the length at $\lambda/8$ at the center frequency. The performance is shown by the solid curves in figure 21. CL_{+2} is independent of frequency as before. CL_{fo} is largely independent of frequency, because the 100-ohm line terminated by a 100-ohm biased diode looks like 100 ohms at all frequencies. Two 100-ohm resistances in parallel at the admittance-adding point give 50 ohms, which exactly matches the input transmission line. CL_{-1} is a function of frequency, again pointing to the dependence of the -1 sideband only on mismatching elements between the diode junctions and the summation point. Setting $Z_{OL} = 100$ ohms and $Z_{OC} = 12.5$ ohms gives the performance shown by the dashed curves in figure 21. As expected, CL_{fo} deteriorated due to the presence of finite Z_{OL}, but CL_{-1} improved, with nonzero Z_{OC} partially compensating for the deterioration caused by the $\lambda/8$ line section.

How much compensation can be achieved by varying Z_{OL} and Z_{OC}? Figure 22 shows CL_{fo} and CL_{-1} for $C_c = 0.2$ pF and $CL_{+1} = 30$ dB for various values of Z_{OL} and Z_{OC}. Again, CL_{fo} was dominated by Z_{OL}, and CL_{-1} was dominated by Z_{OC}. $Z_{OC} = 12.5$ ohms, provided $CL_{-1} \geq 50$ dB (which is 20 dB greater than CL_{+1}) over a 26-percent bandwidth. Increasing Z_{OC} to 50 ohms increased the bandwidth to an octave (0.54 to 1.08 GHz). The length of Z_{OL} should be shortened to prevent CL_{fo} from becoming too small at the high-frequency end.

To determine the relationship between drive power and conversion loss, the simple strip-line structure shown in figure 14 was used with the following diode parameters: $C_d = 0.2$ pF, $C_c = 0.0$ pF, $L_w = 3.7$ nH, $R_s = 2$ ohms, $f_o = 0.675$ GHz, and CL_{fo} was approximately as shown in figure 20 for $Z_{OC} = 12.5$ ohms when the drive gave 10 dB or greater conversion loss. At a drive that should give 0-dB conversion loss, the curve was shifted up in frequency to 0.77 GHz. CL_{+1} versus

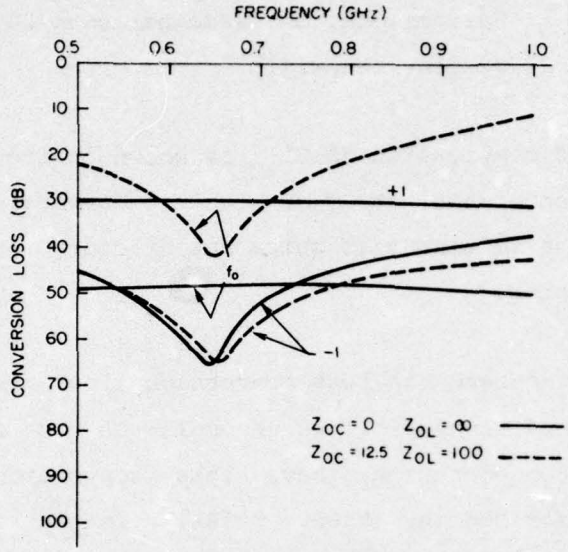

Figure 21. Conversion loss contributions of spacing between diodes.

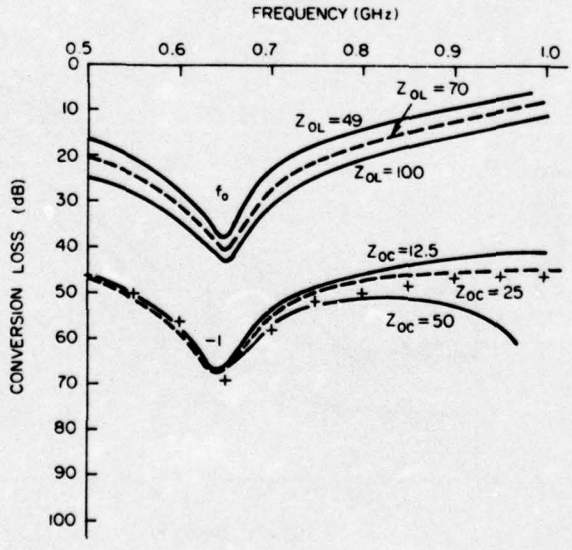

Figure 22. Optimum bandwidth by adjusting Z_{OL} and Z_{OC}.

relative drive is shown in figure 23. S_{-1} tends to remain constant with drive in this simulated circuit up to a drive that should give 10-dB conversion loss. Furthermore, S_{-1} remains about 20-dB up to -10-dB drive over about 25-percent bandwidth.

The gain compression of CL_{+1} is shown in figure 24 for 0.7 GHz. A 1-dB compression occurs at 9-dB desired conversion loss. Thus, the performance of the modulator is quite satisfactory for conversion losses of 10 dB and greater.

The -2 sideband has less conversion loss than the -1 sideband in many cases and always follows the rule $CL_{-2} = 2CL_{+1}$. The other sidebands may, on occasion, have less conversion loss than the -1 sideband, as prescribed by their rules. In an integrator decision circuit, the relative level of the pairs is important, and they are always separated by CL_{fo}.

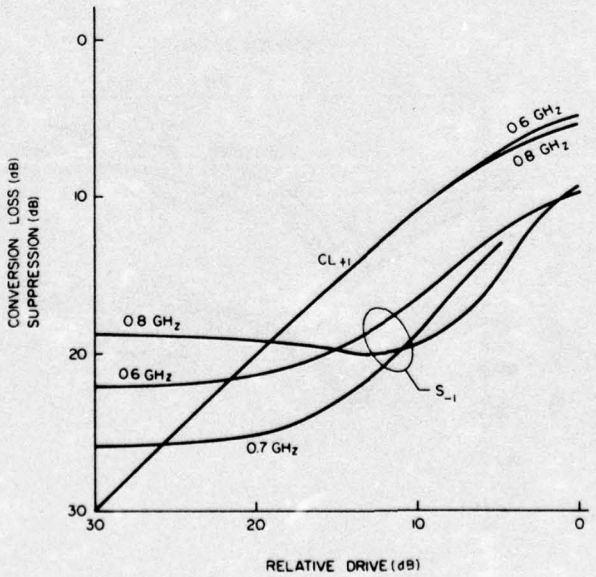

Figure 23. Conversion loss of +1 sidebnad and suppression of -1 sideband.

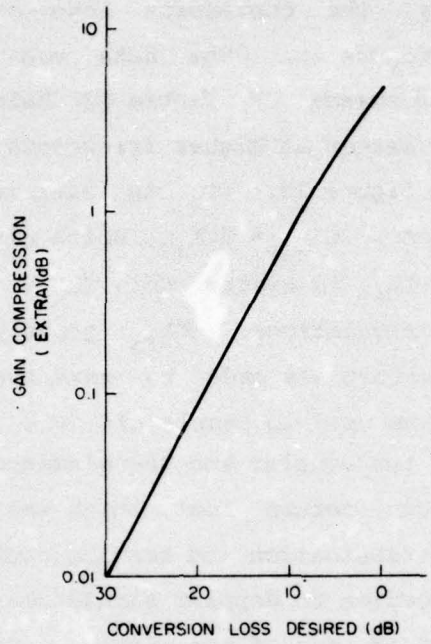

Figure 24. Gain saturation of +1 sideband conversion loss.

3.4 Experimental Results

The SSB modulator shown in figure 14 was evaluated experimentally with the aid of a spectrum analyzer using a 550-kHz frequency offset. Although no capacitance was added to C to make it 0.2 pF instead of 0 pF, the performance should be very much like that in figure 22, in which Z_{OL} = 100 ohms and Z_{OC} = 12.5 ohms. The addition to C_c would increase the conversion loss of the -1 sideband only at the design center frequency. In the computer simulations, the diode biases were adjusted until f_o was suppressed at zero frequency. In the experiments, the diode biases were adjusted to cancel the -1 sideband at the design center frequency, since it is troublesome in the doppler simulator, while f_o is not. Line lengths were selected for 0.65-GHz

design center frequency. The conversion loss of the -1 sideband is shown as curve A in figure 25. The data are quite close to the computer-simulated performance of figure 22 below the design center frequency and slightly better at higher frequencies. All the measurable sidebands are shown in figure 25. CL_{+1} is extremely flat in agreement with computer simulations. $CL_{-2} = 2CL_{+1}$, which also closely agrees with computer simulations. CL_{+1} is greater than CL_{-2}, but not quite so much as predicted in the simulations. CL_{fo} grossly differs from that simulated, because no effort was made to make the device well matched. A directional coupler was used to couple off the reflected power. The finite directivity of the coupler and the mismatches between it and the diodes contributed to the return loss, which was as low as 10 dB up to 1.1 GHz. More careful fabrication and testing could increase the return loss, but in the application to doppler simulation, this return loss is of no consequence. Indeed, one of the advantages of the PIN-diode SSB modulator is that it can be made quite inexpensively and yet perform the doppler simulation function adequately.

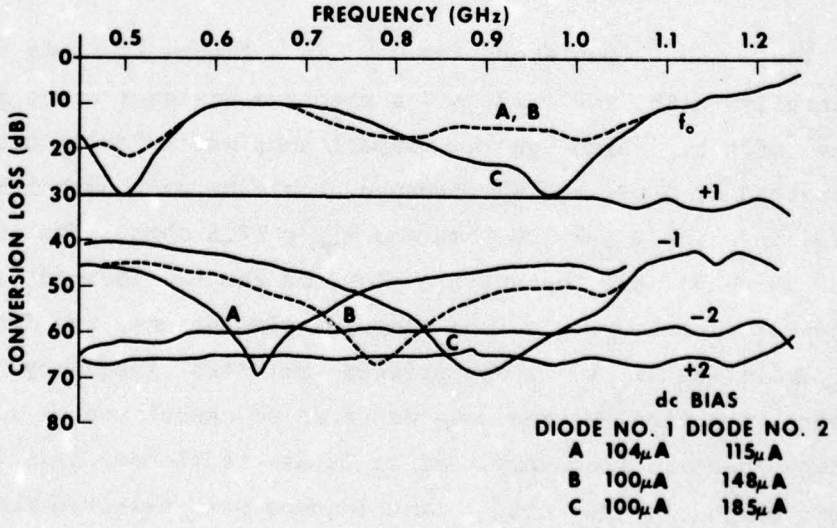

Figure 25. Experimental model performance

Figure 25 shows that the center frequency of operation can be shifted by changing the bias on the farthest diode. Furthermore at bias setting B, $CL_{-1} \geq 50$ dB from 0.65 to 1.04 GHz, which is almost an octave. CL_{+1}, CL_{-2}, and CL_{+2} did not change with bias.

4. DOPPLER TESTER ERRORS

The purpose for developing the $\lambda/8$ PIN-diode SSB modulator is to make use of it in testing altitude sensing fuzes. A fair degree of correlation has been found between pole tests and active firings. But pole tests require rather large equipment, are slow in execution, compromise security information when done out-of-doors, and are not as accurate as desired. Alexander[5] derived an alternative to the pole test, which might be called the minipole test. The fuze sensitivity is derived from the detector voltage waveform just before the fuze antenna comes into contact with a metal ground plane. The technique still provided large errors (in excess of 80 percent) on many fuzes. Wilkin developed a method for measuring the radiated power and sensitivity of a fuze that "has an accuracy of 8%, probably more accurate than a pole test."[6] The method consists of careful measurements of radiated power and sensitivity and equations relating these to function height. The results of the calculations made here indicate that errors using the $\lambda/8$ PIN-diode SSB modulator may be in the $\pm$3-percent range.

---

[5]*Peter Alexander, Induction-Field Determination of Sensitivity for Loop Antenna-Type Fuzes, Harry Diamond Laboratories TM-71-40 (December 1971).*

[6]*Neil D. Wilkin, An Absolute Measurement Procedure to Determine Oscillator-Detector Sensitivity and Power, Harry Diamond Laboratories TR-1606 (April 1972).*

4.1 Tester

From figure 26, the radiated power transmission (beacon) equation gives

$$\frac{P_R}{P_T} = \frac{G_T G_R \lambda^2}{(4\pi R)^2} \quad , \tag{28}$$

in which P_T is the total radiated power, λ is the wavelength, the absorbing plane labeled Γ absorbs nothing, and G_T and G_R are antenna gains over an isotropic radiator. An infinitesimal ideal dipole or loop has a gain of 1.5; a half-wave dipole, 1.64; and an optimum horn, 10 A/λ^2 (in which A is aperture area). For a ground target, the distance to ground will be r = R/2. The ground is assumed to be a lossy reflecting plane with a (voltage) reflection coefficient, between 0 and 1, represented by Γ. For a homodyne system using the same antenna for transmit and receive, $G_T = G_R = G$. For a small, ideally tuned antenna, G = 1.5. Thus, equation (28) becomes

$$\frac{P_R}{P_T} = \left(\frac{1.5\lambda\Gamma}{8\pi r}\right)^2 \quad . \tag{29}$$

The loop loss, α_L, from oscillator to mixer thus becomes

$$\alpha_L = 20 \log \left(\frac{16\pi r}{3\lambda\Gamma}\right) . \tag{30}$$

This loss is shown in figure 27. An additional 10-dB nominal conversion loss of the mixer is assumed to make the total loss from oscillator power to I.F. output power, α_T,

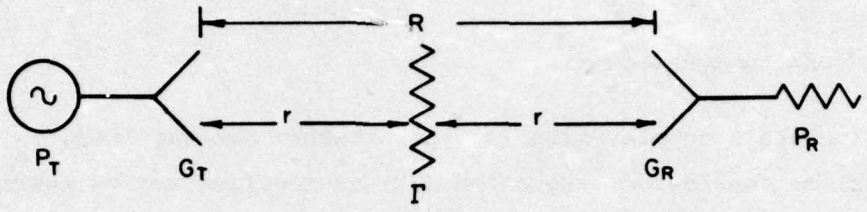

Figure 26. Component arrangement for radiated power transfer equation.

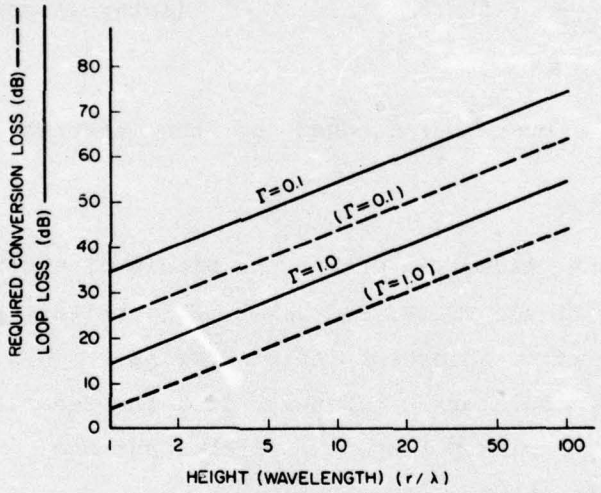

Figure 27. Loop loss and required conversion loss versus height.

$$\alpha_T = 20 \log \left(\frac{16r}{3\lambda\Gamma}\right) \quad . \tag{31}$$

Mismatches between oscillator and antenna may be interpreted as modifying P_T; and between the antenna and mixer, as modifying the conversion loss.

The constant k_1 given in equation (14) for nominal performance is thus

$$k_1 = \frac{3\Gamma}{16} \quad , \tag{32}$$

where $x = r/\lambda$ in equation (14).

To simulate a doppler signal, the external two-way loss, α_E, to the radar must be considered. Equation (29) as modified may be rewritten

$$\frac{P_R}{P_T} = \frac{\Gamma\lambda}{8\pi r} \text{ (external gain)} \times G_T^2 \text{ (internal gain)} \quad . \tag{33}$$

The external gain must be matched by the testing enclosure and modulator.

For testing, the radar is put in the middle of a cubic box 1 λ on a side, as shown in figure 28 (R. McCracken, HDL, private communication). The box is lined with absorbent tiles having $\Gamma \leq 0.1$. A coupling antenna to the SSB modulator is $\Gamma/2$ away from the radar, which may be a waveguide as shown, a pickup loop, or a probe antenna. Therefore, the distance to the test antenna, R_T, is given by

$$R_T = \lambda/2 \quad . \tag{34}$$

By use of equation (28), the gain to the testing modulator, P_m/P_T, is obtained by

$$\frac{P_m}{P_T} = \frac{G_T G_m \lambda^2}{\left(4\pi R_T\right)^2} = \frac{G_T G_m}{(2\pi)^2} \quad , \tag{35}$$

in which G_m is the gain of the tester antenna. The gain from the transmitter to the receiver is the round-trip gain to the modulator,

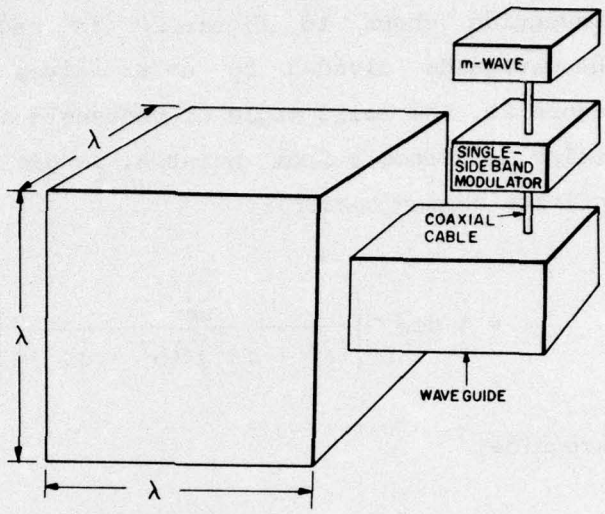

Figure 28. Target simulator box and modulator components.

$$\frac{P_R}{P_T} = \left(\frac{G_m}{4\pi^2}\right)^2 \text{(external gain)} \times G_T^2 \text{ (internal gain)} \; . \quad (36)$$

The round-trip loss to the modulator, α_{RTM}, is thus

$$\alpha_{RTM} = 20 \log \frac{4\pi^2}{G_m} \; . \quad (37)$$

For a small, tuned pickup antenna in the box,

$$G_m = 1.5 \; . \quad (38)$$

Thus,

$$\alpha_{RTM} = 20 \log \frac{8\pi^2}{3} = 28.4 \text{ dB} \; . \quad (39)$$

When the waveguide shown in figure 28 is used, the solid angle subtended by the waveguide divided by 4π sr gives the power gain. Referring to figure 29, the solid angle of rectangle a by b, whose plane is a perpendicular distance ρ from point A, is given by ω (O. Cruzan, formerly HDL, private communication):

$$\omega = 4 \sin^{-1}\left[\frac{ab}{\left(a^2 + 4\rho^2\right)^{\frac{1}{2}}\left(b^2 + 4\rho^2\right)^{\frac{1}{2}}}\right] . \tag{40}$$

In a typical waveguide,

$$a = \lambda/3, \text{ and } b = 3\lambda/4. \tag{41}$$

Recalling that $\rho = \lambda/2$, equation (40) produces

$$\omega = 0.244\pi \quad . \tag{42}$$

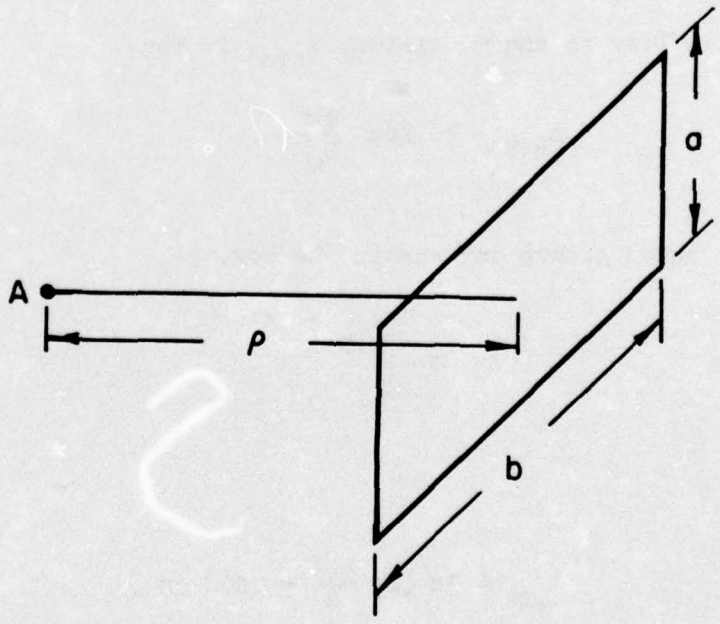

Figure 29. Solid angle of rectangle.

For the waveguide coupler, the round-trip loss to the modulator becomes

$$\alpha_{RTM} = 2 \times 10 \log \frac{4\pi}{0.244\pi} = 24.3 \text{ dB} . \quad (43)$$

About 12-dB one-way loss was measured on an experimental box. If the waveguide were one face of the cube, α_{RTM} would be given by

$$\alpha_{RTM} = 20 \log 6 = 15.6 \text{ dB} . \quad (44)$$

Equations (39), (43), and (44) assume that far-field-radiation power equations are valid at $\lambda/2$, that the radar antenna is radiating in the correct polarization and at maximum gain in the direction of the pickup antenna, and that the radiated power is constant over the effective area of the pickup antenna.

The external attenuation in field use, α_E, of equation (33) must be matched by the round-trip loss to the modulator, α_{RTM}, and the modulator conversion loss to the desired sideband, CL_{+1}.

$$\alpha_E = CL_{+1} + \alpha_{RTM} . \quad (45)$$

Thus,

$$CL_{+1} = \alpha_E - \alpha_{RTM} = 20 \log \frac{8\pi r}{\Gamma\lambda} = 24.3 \text{ dB} . \quad (46)$$

Assuming a ground return down 20 dB, then $\Gamma = 0.1$, and

$$\begin{aligned} CL &= 20 \log 80\pi - 24.3 \text{ dB} + 20 \log (r/\lambda) \\ &= 23.7 \text{ dB} + 20 \log (r/\lambda), \end{aligned} \quad (47)$$

which is shown as the dashed lines in figure 27. Use of coupling loop or probe pickup antennas would lower the required conversion loss (figure 27 by 4.1 dB.

Even if the SSB modulator reflected all the incident transmitter power (f_o) impinging on it, α_{RTM} would reduce it by 24 to 28 dB, making it lower than the power reflected by the tiles lining the box walls, which is about 20 dB down.

4.2 Comparative Errors

The error in function height due to the undesired sidebands of the PIN-diode SSB modulator is here compared with the errors introduced by other mixer-type and serrodyne SSB modulators. It is assumed that all bandwidth problems have been solved with the other modulators and that the additional circulator and variable attenuator required do not contribute to errors. These other modulators normally have many undesired sidebands with $S_{-1} = S_{-2} = S_{+2}$, as have been observed, and to simplify comparison, it is assumed that all other undesired sidebands do not exist. As shown in sections 2.1.2 and 4.1, CL_{fo} does not contribute to system response for most systems and therefore is ignored.

Since the return loss of the ground varies between 20 and 0 dB, 10 dB ($\Gamma = 0.316$) is assumed for comparison. Ten wavelengths are assumed as a typical function height. From equation (46), CL ≃ 34 dB was required.

As shown in figure 25, the best performance is obtained by designing the PIN modulator to work at a lower frequency than desired and adjusting the bias for it to work at the desired higher frequency. (A similar result was obtained in computer simulations by adjusting characteristic impedances, as shown in figure 22.) From figure 25, f_o

is taken as 0.9 GHz, and the other frequencies are normalized to it. Figure 23 shows that S_{-1} does not change much with CL_{+1}. $CL_{+2} \simeq CL_{-2}$ + 6 dB rather than $CL_{+2} = CL_{-2} + CL_{fo}$, as given in equation (25).

The undesired sidebands make their contribution to error by modifying the effective oscillator power level. The -1 sideband adds or subtracts directly (in voltage). The +2 and -2 sidebands are combined to give their maximum and minimum; their effective contribution to the S_{-1} sideband is then determined by use of figure 11. (It is anticipated that higher-order sidebands make the same contribution to S_1, as shown in figure 11.) Thus, the normalized magnitude of oscillator voltage k_2 determines the error directly. The normalized voltage at the peak detector is given by

$$V_D = k_2 \frac{k_1}{h} \quad , \tag{48}$$

which is similar to equation (17) (no integral operation and no threshold subtracted). The term h_o is defined as the desired function height when $k_2 = 1$. Then

$$V_D = k_2 \frac{k_1}{h} = \frac{k_1}{h_o} \quad , \quad \frac{h}{h_o} = k_2 \quad . \tag{49}$$

Thus, $k_2 = 1.1$ gives +10-percent error, and $k_2 = 0.9$ gives -10-percent error for the peak detectors.

For integration decision circuits, k_2 multiples $1/x$ in equation (16) before integration and produces

$$V_i = k_1 \frac{2}{\pi} \left(\frac{h}{H} - 1 + k_2 \ln \frac{H}{h} \right). \tag{50}$$

Equating the voltage with error (k_2 and h) to the nominal response without error ($k_2 = 1$ and $h = h_o$),

$$V_i = k_1 \frac{2}{\pi} \left(\frac{h}{H} - 1 + k_2 \ln \frac{H}{h} \right) = k_1 \frac{2}{\pi} \left(\frac{h_o}{H} - 1 + \ln \frac{H}{h_o} \right). \tag{51}$$

Since

$$\frac{h}{H} \leq \frac{h_o}{H} << 1 ,$$

then

$$k_2 \ln \frac{H}{h} = \ln \frac{H}{h_o} , \tag{52}$$

which leads to

$$\frac{h}{h_o} = \left(\frac{H}{h_o} \right)^{(k_2 - 1)/k_2} \tag{53}$$

for integration decision circuits.

The maximium errors of the PIN-diode and mixer (other) SSB modulators can be compared in figure 30. Changing to $\Gamma = 0.1$ moves only the positive error PIN-diode peak detecting curve. The entire curve shifts down 2.5 percent.

An example at one frequency shows how figure 30 was derived. For the PIN-diode SSB modulator, S_{-1} = 20 dB at 0.73 GHz (f/f_o = 0.81). From above, CL = 34 dB = S_{-2}, and S_{+2} = 34 + 6 = 40 dB. Therefore, V_{-1}/V_{+1} = 0.1, V_{-2}/V_{+1} = 0.02, and V_{+2}/V_{+1} = 0.01.

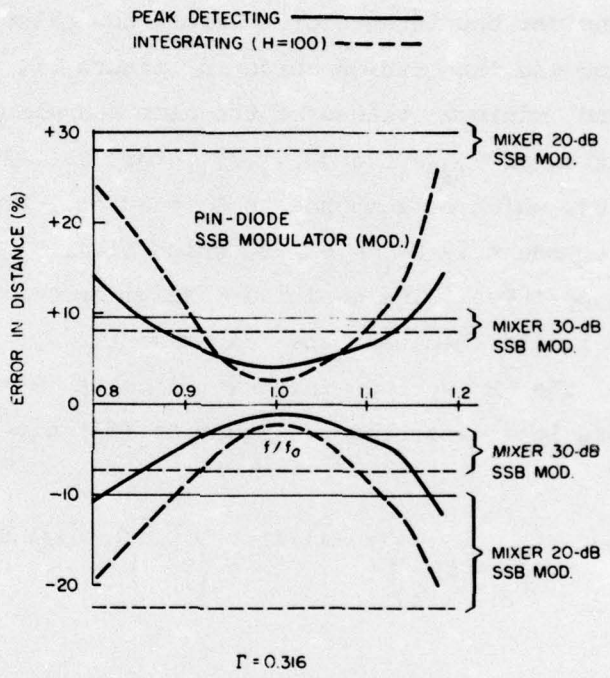

Figure 30. Distance error comparison for single-sideband modulators.

The maximum of these voltages is 0.13; thus by use of equation (49), h/h_o = 0.13, and the maximum positive error is +13 percent for peak detection. Since the ±2 sidebands always increase effective oscillator power (fig. 8), the maximum negative error is due to the -1 sideband subtracting its maximum and the ±2 sidebands adding their least. They are at their least when they are out of phase, which gives $|0.02 - 0.01| = 0.01$. Then 0.01 gives S_2 = 40 dB, and using figure 11 for minimum peak gives equivalent S_{-1} = 60 dB, V_{-1}/V_{+1} = -0.1 + 0.001 = -0.099, and h/h_o = 0.901, giving the maximum negative error of -9.9 percent.

For the mixer modulator, $S_{-1} = S_{-2} = S_{+2} = 20$ dB is considered. $V_{-1}/V_{+1} = V_{-2}/V_{+1} = V_{+2}/V_{+1} = 0.1$. The maximum positive value is 0.3, which gives +30 percent. Since $V_{-2} = V_{+2}$, they can at worst cancel, so maximum negative normalized voltage is -0.1, which provides -10 percent.

Now consider the integrator. Error is calculated by use of equation (53) and the integration curve in figure 11, which is used for both maximum and minimum values of the plus and minus sidebands. The maximum combination of V_{-2}/V_{+1} and V_{+2}/V_{+1} for the PIN-diode modulator is $V_{+2}/V_{+1} = 0.03$, which corresponds to $S_2 = 30$ dB. From figure 11, the equivalent -1 component is $S_{-1} = 60$ dB, which gives $V_{-1}/V_{+1} = 0.001$, and this must be positive. The positive maximum becomes $V_{-1}/V_{+1} = 0.101$; therefore, $k_2 = 1.101$. Because the experimental points in figure 10 were close to the H = 100 integration curve, H = 100 is used for estimating errors in an integrator. Equation (53) gives

$$\frac{h}{h_o} = \left(\frac{H}{h_o}\right)^{(k_2-1)/k_2} = \left(\frac{100}{10}\right)^{0.101/1.101} = 1.232 \quad , \quad (54)$$

which gives +23.2-percent error for the integrator and PIN-diode SSB modulator. For the maximum negative error, the equivalent V_{-1}/V_{+1} from the ±2 sidebands is even smaller, and k = 0.9, which provides $h/h_o = 0.813$, giving -18.7-percent error.

For the mixer modulator, $V_{-2}/V_{+1} + V_{+2}/V_{+1} = 0.2$, which corresponds to $S_2 = 14$ dB. From figure 11, $S_{-1} = 34$ dB, giving $V_{-1}/V_{+1} = 0.02$. The effective k = 1.12 gives $h/h_o = 1.280$ and thus provides +28.0-percent error. The maximum negative addition of voltages provides k = 0.9, which makes $h/h_o = 0.774$, giving -22.6-percent error.

The calculations as shown in figure 30 indicate that over a 30-percent bandwidth, the PIN-diode SSB modulator is superior to a mixer modulator having 20-dB suppression of undesired sidebands and superior over a 15-percent bandwidth to a mixer modulator having 30-dB suppression of undesired sidebands when used for testing the function height of peak or integration decision-circuit doppler radars. The error at f_o for integrators with the PIN-diode SSB modulator is less than ±3 percent; and for peak detectors, +4 and -2 percent. The +4 percent is a function of simulated height (or Γ) and tends to remain a constant error of 0.4λ as height is changed (or equivalent Γ; see fig. 27).

5. CONCLUSIONS

The sideband requirements for modulators for testing simple doppler radars have been derived. The PIN-diode SSB modulator satisfies these requirements much better and less expensively than conventional mixer or serrodyne SSB modulators. Furthermore, the PIN diode may be attached directly to the tester box without an additional circulator and variable attenuator. The sideband requirements used in the past are not realistic. Carrier suppression is not important, and the -1 sideband is the most important of all. All other sidebands are also important if their suppression does not increase rapidly away from the carrier frequency.

LITERATURE CITED

(1) Raymond C. Cumming, The Serrodyne Frequency Translator, Proc. IRE, 45 (February 1957), 175-186.

(2) Robert V. Garver, 360° Varactor Linear Phase Modulator, IEEE Trans. Microwave Theory and Techniques, MTT-17 (March 1969), 137-147.

(3) Gerald Klein and Leonard Dubrowsky, The Digilator, A New Broadband Microwave Frequency Translator, IEEE Trans. Microwave Theory and Techniques, MTT-15 (March 1967), 172-179.

(4) B. N. Schiffman, A New Class of Broad-Band Microwave 90-Degree Phase Shifters, IRE Trans. Microwave Theory and Techniques, MTT-6 (April 1958), 232-237.

(5) Peter Alexander, Induction-Field Determination of Sensitivity for Loop Antenna-Type Fuzes, Harry Diamond Laboratories TM-71-40 (December 1971).

(6) Neil D. Wilkin, An Absolute Measurement Procedure to Determine Oscillator-Detector Sensitivity and Power, Harry Diamond Laboratories TR-1606 (April 1972).

APPENDIX A.--DERIVATION OF DOPPLER MIXER OUTPUT APPROXIMATION

The direct wave incident on a doppler mixer is given by

$$V_{LO} e^{j\omega_o t} \quad ,$$

in which ω_o is the oscillator frequency. The indirect wave (reflected off a target) will have a much smaller voltage, V_{sig}, and will be delayed in phase by θ, giving

$$V_{sig} e^{j(\omega_o t+\theta)} \quad .$$

The output of the mixer is the sum of these as reduced by the conversion loss k:

$$V_{mix} e^{j\omega_o t} = k\left(V_{LO} e^{j\omega_o t} + V_{sig} e^{j(\omega_o t+\theta)}\right)$$

$$V_{mix} = k\left(V_{LO} + V_{sig}\, e^{j\theta}\right)$$

$$= k\left(V_{LO} + V_{sig} \cos\theta + jV_{sig} \sin\theta\right)$$

$$\left|V_{mix}\right| = k\left[\left(V_{LO} + V_{sig} \cos\theta\right)^2 + \left(V_{sig} \sin\theta\right)^2\right]^{\frac{1}{2}}$$

$$\left|V_{mix}\right| \approx k\left(V_{LO} + V_{sig} \cos\theta\right)$$

for $V_{sig} \ll V_{LO}$.

DISTRIBUTION

DEFENSE DOCUMENTATION CENTER
CAMERON STATION, BUILDING 5
ALEXANDRIA, VA 22314
ATTN DDC-TCA (12 COPIES)

COMMANDER
USA RSCH & STD GP (EUR)
BOX 65
FPO NEW YORK 09510
ATTN LTC JAMES M. KENNEDY, JR.
CHIEF, PHYSICS & MATH BRANCH

COMMANDER
US ARMY MATERIEL DEVELOPMENT & READINESS COMMAND
5001 EISENHOWER AVENUE
ALEXANDRIA, VA 22333
ATTN DRXAM-TL, HQ TECH LIBRARY

COMMANDER
USA ARMAMENT COMMAND
ROCK ISLAND, IL 61201
ATTN DRSAR-ASF, FUZE DIV
ATTN DRSAR-RDF, SYS DEV DIV - FUZES

COMMANDER
USA MISSILE & MUNITIONS CENTER & SCHOOL
REDSTONE ARSENAL, AL 35809
ATTN ATSK-CTD-F

PROJECT MANAGER
PATRIOT PROJECT OFFICE
USA DARCOM
REDSTONE ARSENAL, AL 35807
ATTN DRCRM-MD-T-EG

PATRICK FIELD OFFICE
WHITE SANDS MISSILE RANGE, NM 88002
ATTN LT. C. W. DONNER

OFFICE OF MISSILE ELECTRONICS WARFARE
WHITE SANDS MISSILE RANGE, NM 88002
ATTN CHIEF, DRSEL-WLM-MF
ATTN A. NORTE

THE BENDIX CORPORATION
COMMUNICATION DIVISION
EAST JOPPA RD-TOWSON
BALTIMORE, MD 21204

IBM CORPORATION
150 SPARKMAN DR. NW
HUNTSVILLE, AL 35805
ATTN MR. WOOD

MARTIN MARIETTA AEROSPACE
ORLANDO DIVISION
PO BOX 5837
ORLANDO, FL 32805

RAYTHEON COMPANY
HARTWELL ROAD
BEDFORD, MA 01730
ATTN FRED FIRST

RAYTHEON COMPANY
WHITE SANDS MISSILE RANGE, NM 88002
ATTN C. PHILPOTT

HARRY DIAMOND LABORATORIES
ATTN MCGREGOR, THOMAS, COL, COMMANDING
OFFICER/FLYER, I.N./LANDIS, P.E./
SOMMER, H./CONRAD, E.E.
ATTN CARTER, W.W., DR., ACTING TECHNICAL
DIRECTOR/MARCUS, S.M.
ATTN KIMMEL, S., IO
ATTN CHIEF, 0021
ATTN CHIEF, 0022
ATTN CHIEF, LAB 100
ATTN CHIEF, LAB 200
ATTN CHIEF, LAB 300
ATTN CHIEF, LAB 400
ATTN CHIEF, LAB 500
ATTN CHIEF, LAB 600
ATTN CHIEF, DIV 700
ATTN CHIEF, DIV 800
ATTN CHIEF, LAB 900
ATTN CHIEF, LAB 1000
ATTN RECORD COPY, BR 041
ATTN HDL LIBRARY (3 COPIES)
ATTN CHAIRMAN, EDITORIAL COMMITTEE
ATTN CHIEF, 047
ATTN TECH REPORTS, 013
ATTN PATENT LAW BRANCH, 071
ATTN MCLAUGHLIN, P.W., 741
ATTN CHIEF, 610
ATTN GARVER, R., 1010 (10 COPIES)